

Article

Nd-Sr Isotopic Study of Magmatic Rocks and $^{40}\text{Ar}/^{39}\text{Ar}$ Dating of the Mafic Dike of the Proterozoic Ulan-Sar'dag Ophiolite Mélange (Southern Siberia, East Sayan, Middle Belt, Russia)

Olga Kiseleva ^{1,*}, Pavel Serov ² , Evgenia Airiyants ¹, Aleksey Travin ¹ , Dmitriy Belyanin ¹ , Brain Nharara ¹  and Sergey Zhmodik ¹

¹ Sobolev Institute of Geology and Mineralogy, Siberian Branch of the Russian Academy of Sciences, 630090 Novosibirsk, Russia; jenny@igm.nsc.ru (E.A.); travin@igm.nsc.ru (A.T.); bel@igm.nsc.ru (D.B.); briantnharara@gmail.com (B.N.); zhmodik@igm.nsc.ru (S.Z.)

² Geological Institute of the Kola Science Centre, Russian Academy of Sciences, 184209 Apatity, Russia; serov@geoksc.apatity.ru

* Correspondence: kiseleva_on@igm.nsc.ru; Tel.: +79-83-126-7072

Abstract: We report the first radiogenic Nd-Sr isotope data in the magmatic rocks island-arc ophiolite assemblage from the middle branch of the East Sayan ophiolite complexes to better constrain geodynamic processes in this segment of the CAO in southern central Siberia. The magmatic rocks belong to the following geochemical types: (1) Ensimatic island-arc boninites; (2) island-arc assemblage; (3) enriched basalts of mid-ocean ridges; and (4) oceanic island-like basalts. The boninites have a positive value $\epsilon\text{Nd}(T)$, which is generated from a depleted mantle source (N-MORB). The island-arc assemblage has negative or slightly positive $\epsilon\text{Nd}(T)$ and was formed from an enriched mantle source due to the subduction of terrigenous rocks. The source of the terrigenous material was most likely the rocks of the Archean TTG (Trondhjemite Tonalite Granodiorite) complex of the Gargan block. Isotopic ratios for E-MOR and OIB-like basalts are characterized by positive or slightly negative values of $\epsilon\text{Nd}(T)$. The mafic dike, which crosscut ophiolite rocks, corresponds to OIB-like basalts. The values of $\epsilon\text{Nd}(T)$, measured $^{87}\text{Sr}/^{86}\text{Sr}$ and $I(\text{Sr})$, in the mafic dike correspond to the EM I mantle source. The E-MOR and OIB-like basalts appear to be formed in late-stage asthenospheric mantle melting via the decompression melting processes. The obtained isotope geochemical data for the E-MOR and OIB-like basalts probably indicate the mixing of island-arc melts with asthenospheric melts. We undertook $^{40}\text{Ar}/^{39}\text{Ar}$ dating of the mafic dike, which crosscut the ophiolite unit. The mafic dike has a whole-rock $^{40}\text{Ar}/^{39}\text{Ar}$ weighted mean plateau age of 799 ± 11 Ma. The dating constrains the minimum age of the ophiolite and island-arc magmatism in the region.

Keywords: Southern Siberia; CAO; mantle sources; island-arc assemblage; Nd-Sr isotope geochemistry; $^{40}\text{Ar}/^{39}\text{Ar}$ dating



Citation: Kiseleva, O.; Serov, P.; Airiyants, E.; Travin, A.; Belyanin, D.; Nharara, B.; Zhmodik, S. Nd-Sr Isotopic Study of Magmatic Rocks and $^{40}\text{Ar}/^{39}\text{Ar}$ Dating of the Mafic Dike of the Proterozoic Ulan-Sar'dag Ophiolite Mélange (Southern Siberia, East Sayan, Middle Belt, Russia). *Minerals* **2022**, *12*, 92. <https://doi.org/10.3390/min12010092>

Academic Editors: Koen De Jong and Federica Zaccarini

Received: 18 November 2021

Accepted: 11 January 2022

Published: 14 January 2022

Publisher's Note: MDPI stays neutral with regard to jurisdictional claims in published maps and institutional affiliations.



Copyright: © 2022 by the authors. Licensee MDPI, Basel, Switzerland. This article is an open access article distributed under the terms and conditions of the Creative Commons Attribution (CC BY) license (<https://creativecommons.org/licenses/by/4.0/>).

1. Introduction

The studied area is located in the southeastern region of Eastern Sayan, southern Siberia (the Buryatia Republic of the Russian Federation). This region was tectonically juxtaposed during the Neoproterozoic accretionary orogeny of the Central Asian Orogenic Belt (CAOB), which consists of a complex amalgamation of geologic terranes comprising rocks of Archean to Mesozoic ages [1–7]. The earliest stages in the CAOB formation are related to the development of the Paleo-Asian Ocean [2–5,8–13].

Continental rifting, ocean subduction, and marginal basin formation events began before 1000 Ma and continued until 570 Ma [7]. During the early Paleozoic to late Mesozoic periods, the island arcs, ophiolites, oceanic islands, seamounts, accretionary wedges, oceanic plateau, and microcontinents were joined to the Siberian craton [2,7,14,15] (Figure 1). The southeastern domain of the CAOB includes Archean-Proterozoic terranes—Gargan

block (microcontinent) [2,10,16,17], Proterozoic platform carbonate cover (Irkut suites) [18], ophiolite complexes, and Paleozoic terranes: Khamardaban and Khamsara belts (Figure 2). Several tectonically dismembered ophiolite complexes are exposed along the margin of the Gargan block and tectonically thrust over this block [5,6,19–23]. The studied ophiolitic complexes are Southern Siberia’s largest and best-preserved relics of the ancient oceanic crust of the Paleo-Asian ocean and formed three ophiolitic branches (Figure 2). Recent studies have discussed that the Proterozoic East Sayan ophiolites were formed under different geodynamic regimes. Generally, geochemical signatures for the magmatic rocks associated with Eastern Sayan ophiolites reveal a wide compositional series: mid-ocean ridge basalt (MORB)-type basalts (tholeiites), boninites, island-arc andesites and dacites, and ocean island basalt (OIB)-type basaltic rocks. There are numerous isotopic data of the island arc assemblage and ophiolites in a different segment of CAO, but isotope geochemical data of Proterozoic Eastern Sayan ophiolites are limited [4,20–34].

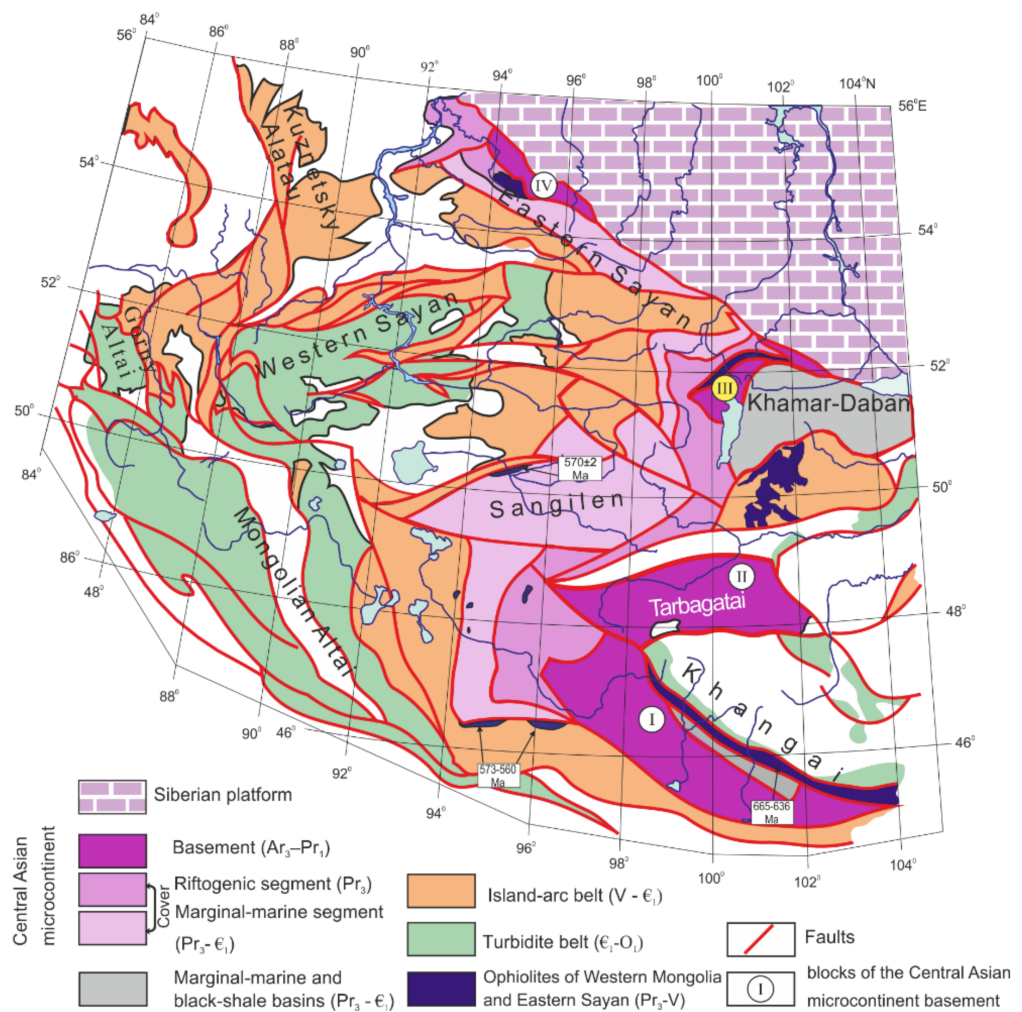


Figure 1. The modern structure of the Central Asian mobile belt by [35,36]. I–IV—blocks of the Central Asian microcontinent basement (I—Baidarik massif, II—Tarbagatai massif, III—Gargan massif, IV—Kansk massif). The studied region is located in the III—Gargan massif.

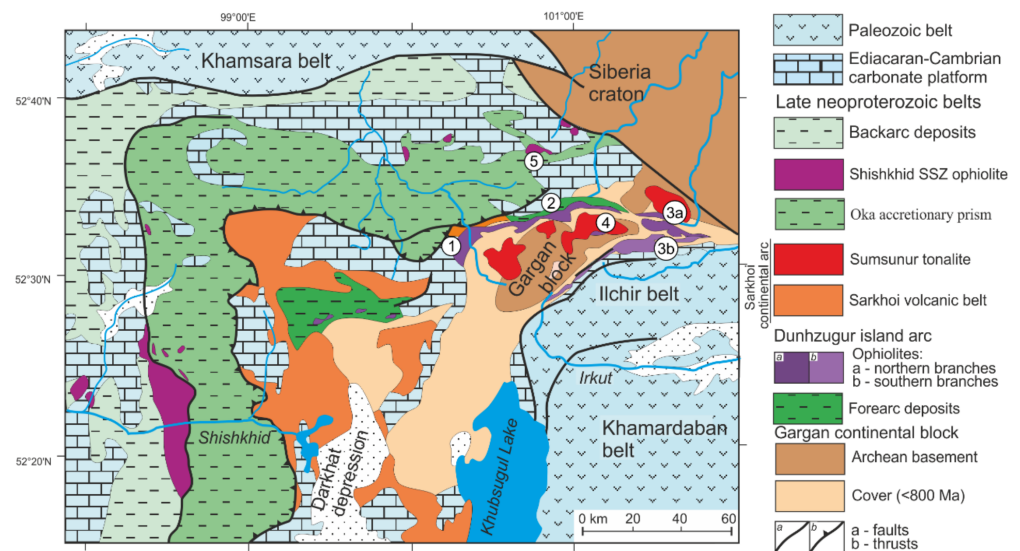


Figure 2. Major geological units of eastern Tuva–Sayan, modified from [37] with new information from the authors [26]. Captions of the ophiolite massifs: 1—Dunzhugur, 2—Holbin-Hairhan, 3a—northern branch of Ospa–Kitoi, 3b—southern branch of Ospa–Kitoi, 4—Ulan-Sar’dag, 5—Ehe-Shigna Shishkhid branch.

The Ulan-Sar’dag ophiolite mélangé (for simplicity called Ulan-Sar’dag massif—USM) belongs to the middle and possibly independent ophiolitic branch [34]. Magmatism of the studied area has been controlled by the evolution of the island arc and subduction zone. Isotope geochemical studies of the Ulan-Sar’dag massif will provide important information about mantle sources, mantle–crust interaction, and the evolution arc magmatism in the studied segment of the CAOB.

Based on the geochemical data, we recently discussed the Ulan-Sar’dag massif composed of magmatic rocks with different geochemical signatures [26], which formed due to multistage magmatism, according to the evolution of the subduction zone in the studied segment of CAOB.

This work aimed to study the Sr-Nd isotope characteristics for each geochemical type’s rocks of the Ulan-Sar’dag massif. Radiogenic Sr-Nd isotopic and trace elements geochemistry should display contributions of different magmatic sources and melts, mantle–crust interaction, and metamorphic processes. We also determined the ages of the mafic dike, which crosscuts the ophiolites, by the $^{40}\text{Ar}/^{39}\text{Ar}$ geochronology method that constrains the minimum age of the ophiolite in the region implying that all accretion ended in the early Neoproterozoic (late Tonian). The isotope geochemical and some geochronological data offer the opportunity to better constrain geodynamic processes in this segment of the CAOB in southern central Siberia.

2. Geological Settings

The Ulan-Sar’dag massif is located in the inner part of the Gargan block (Figure 2). The north ophiolite branch includes the Dunzhugur massif, situated at the Gargan block’s western margin, and the northern part of the Ospa–Kitoi massif (Figure 2). The Dunzhugur ophiolite assemblage is associated with the same name Dunzhugur island-arc complex and two generations of basic dikes, intruding of the Dunzhugur ophiolite [20,29]. The plagiogranite and volcanoclastic rocks in the Dunzhugur island-arc complex yielded an age of 1020–850 Ma [4,20,21] using U-Pb and Pb/Pb zircon dating. The evolution of the Dunzhugur island-arc complex continued during the period of 850–760 Ma [4,20,21]. A collision of the Dunzhugur island arc and the continental margin of the Gargan block occurred at about 810 Ma [4].

The south ophiolite branch includes the southern part of the Ospa–Kitoi massif. At the Ospa–Kitoi, ophiolitic serpentinite mélangé is unconformably overlain by dolomites of the Gorlyk suite, with a late Neoproterozoic–early Cambrian age with the contact between them marked by ophiocalcites [4,6,8]. It is the only stratigraphic evidence for a late Neoproterozoic age of the ophiolitic assemblage.

The ophiolite assemblage of the Ulan-Sar’dag massif (USM) is associated with the volcanic–sedimentary sequence (Ilchir suite), Proterozoic Carbonate Cover (Irkut suite), syn-collisional Sumsunur tonalite–trondhjemite complex with an age of 790 Ma [19] (Figure 3). The ophiolite assemblage and volcanic–sedimentary sequence are presented as independent tectonic slices. The units are tectonically obducted on the Gargan block. The age of the trachyandesite from the volcanogenic sequence of the USM determined by U-Pb dating of the zircon is 833 ± 4 Ma [26]. The Ulan-Sar’dag massif is a lenticular body elongated in an east–west direction with dimensions of 2×5 km². It occurs as an ophiolitic mélangé, composed of various structurally mixed different ages, origins, lithostratigraphic units. These units are represented by ophiolitic altered ultramafic–mafic rocks with podiform chromitites, foliated serpentinites, deep sea sedimentary cherts, shaled volcanic–sedimentary (Ilchir suite) rocks with MORB, island-arc and OIB-like geochemical affinities, mafic dikes, and limestones (Irkut suite) (Figures 3 and 4) [24–26]. The volcanic–sedimentary slice is composed of two units: lower—metavolcanic unit and upper—black, black-quartz-carbonate schists and marbles. The volcanic–sedimentary slice is thrust on the cover limestones of the Irkut suite. The ophiolite slice is thrust on the volcanic–sedimentary units. The rocks at the base of the tectonic ophiolite slice are intensively deformed and have numerous shear zones and sliding surfaces. The thrust zone is marked by foliated serpentinite (Figure 4). On the eastern flank of the Ulan-Sar’dag massif, the mafic dikes crosscut the ophiolite unit (Figure 4). Dikes have a northeastern extension, with a length of 650–700 m and a thickness of up to 10 m (azimuth 320–330°, angle 75°). At the border with the dunite, chilled margins exist with a thickness of up to 1.5 m.

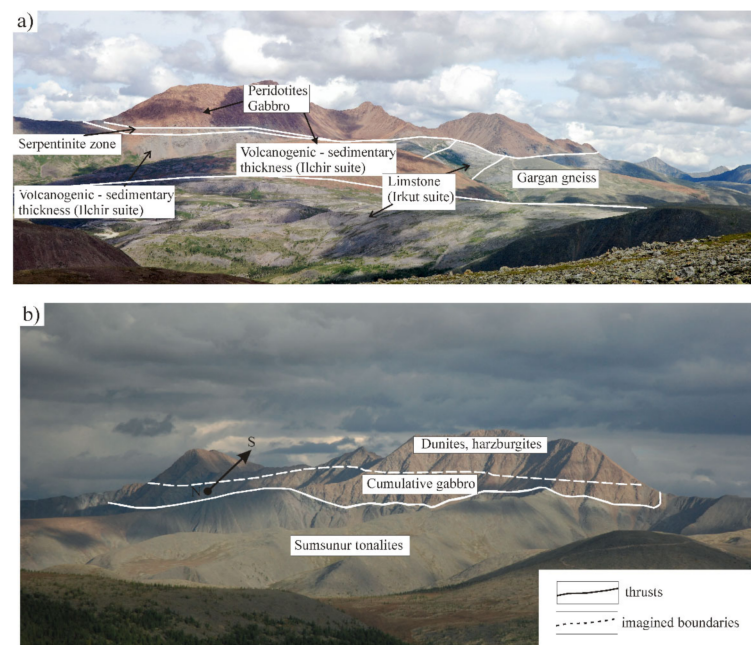


Figure 3. Photographs of field relationship between the mantle peridotites and volcanic–sedimentary sequence (Ilchir suite), limestone (Irkut suite), Gargan gneisses, and Sumsunur tonalites [26]. (a) view at the south side of the Ulan-Sar’dag massif (USM) and (b) view at the north side of the Ulan-Sar’dag massif.

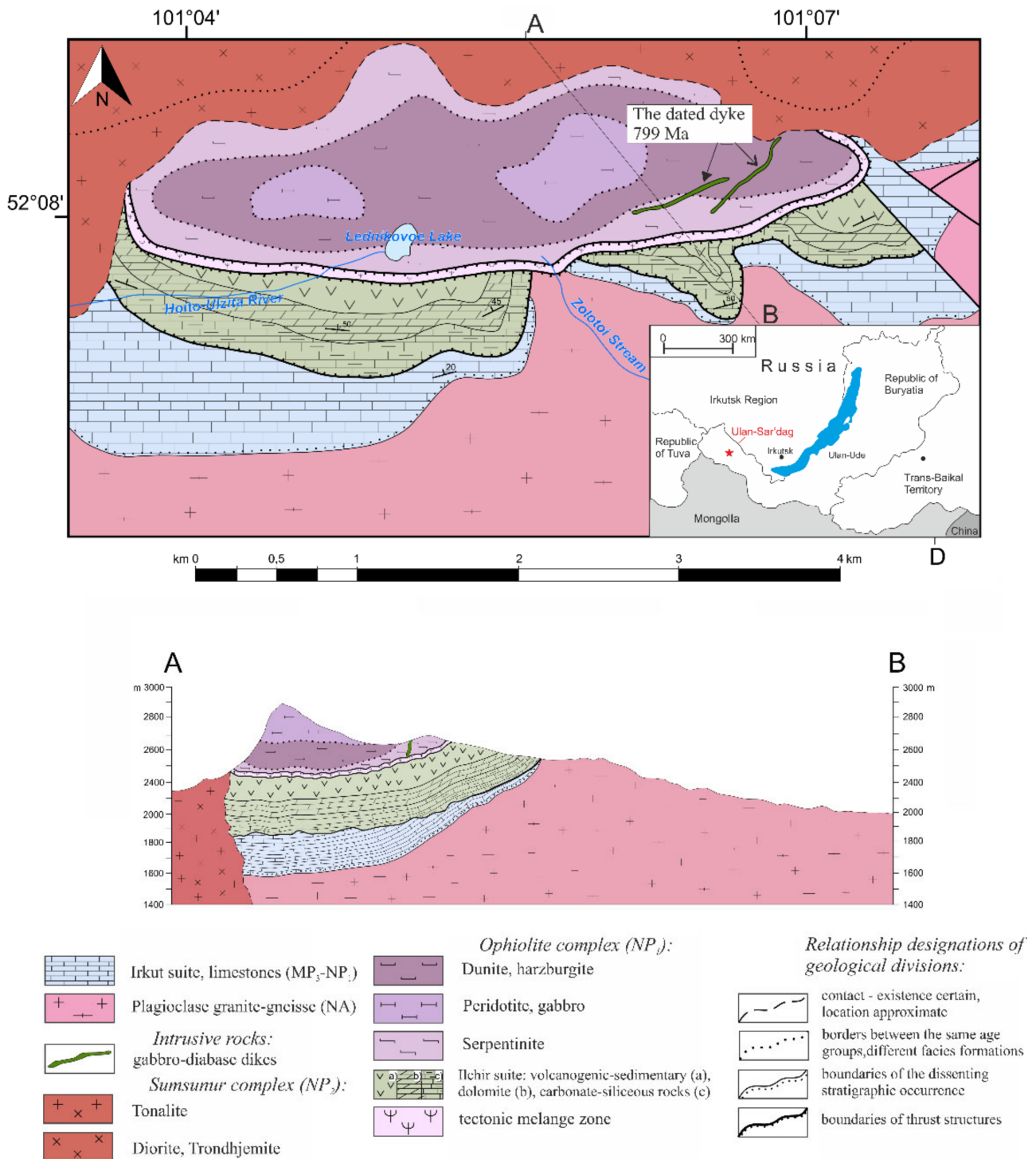


Figure 4. Geological scheme of the Ulan-Sar'dag massif.

3. Materials and Methods

3.1. Sample Description

The ophiolite rocks and the lower units of the volcanic–sedimentary sequence (Ilchir suite) were studied in term geochemistry [26] and isotope characteristics.

The studied rocks are strongly affected by alteration and metamorphic processes. The mantle peridotites are mainly serpentized. The cumulate rocks include amphibolized pyroxenite and gabbro. These consist mainly of amphibolized pyroxenites, isotropic amphibolized gabbros, rare olivine-bearing pyroxenites. Metamorphosed volcanic (metavolcanic)

rocks have a chemical composition corresponding to basalt, trachybasalt, basaltic-andesite, andesite, trachyandesite, and dacite (Figure 5). Detailed petrographic and geochemical characteristics of rocks are given in the previous work [26].

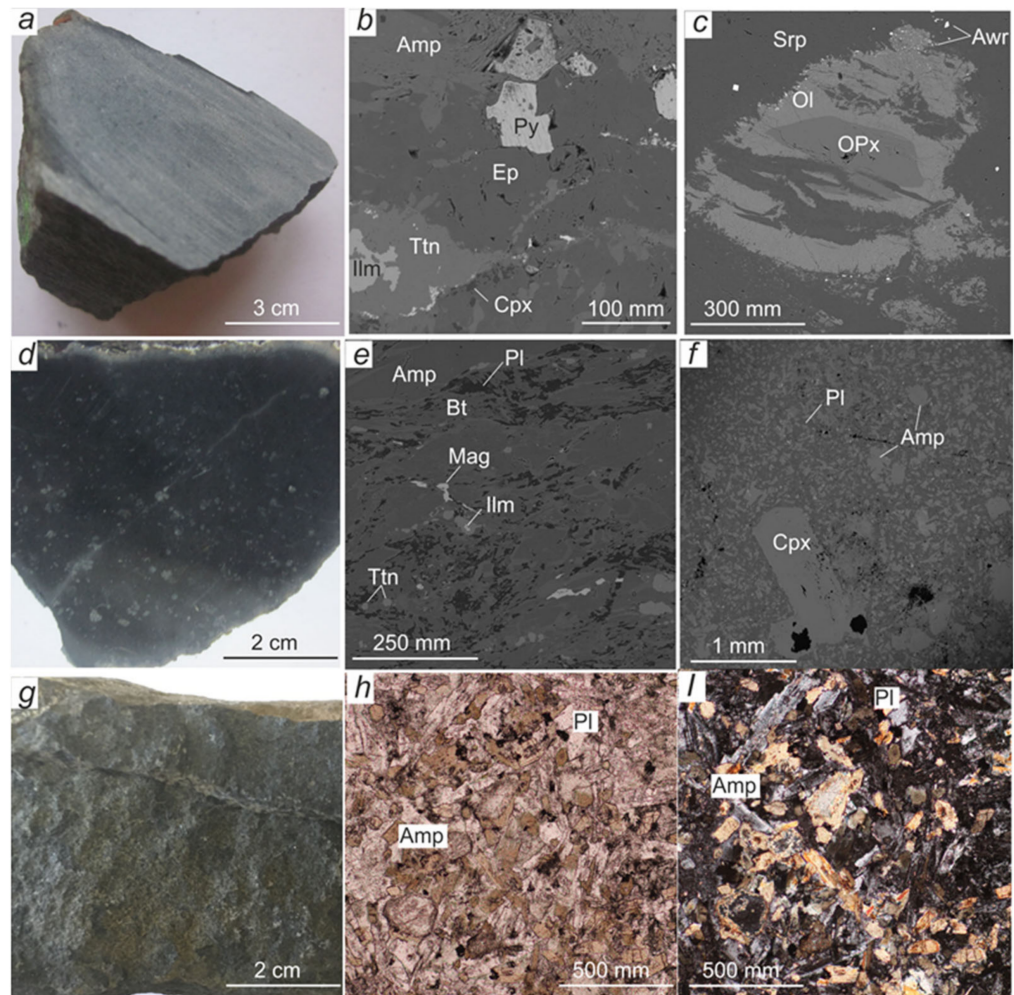


Figure 5. Photos, backscattered electron (BSE) and photomicrographs in cross- and plane-polarized light microphotographs of some samples from the Ulan-Sar'dag massif [26]: (a–c) olivine-bearing amphibolized pyroxenite—olivine phenocrysts with orthopyroxene inclusion in an olivine-amphibole-plagioclase-talc-serpentine matrix, plagioclase replaced by epidote; (d–f) amphibolized gabbro with porphyritic texture; (g–i) basalt's fine-grained structure with a hypidiomorphic aphanitic texture of groundmass consisting of amphibolitized pyroxene and laths of subidiomorphic plagioclase. Abbreviations: Ol—olivine, Opx—orthopyroxene, Cpx—clinopyroxene, Amp—amphibole, Pl—plagioclase, Bt—biotite, Mag—magnetite, Srp—serpentine, Ap—apatite, Ep—epidote, Ilm—ilmenite, Ttn—titanite, Awr—awaruite.

The analyses of the whole-rock major, trace, and rare-earth element compositions were carried out at the Analytical Center for Multi-Elemental and Isotope research (VS Sobolev Institute of Geology and Mineralogy, Novosibirsk, Russia). According to major and trace element compositions, four geochemical types of the magmatic rocks were identified in the area of the USM. The types are (1) boninites; (2) island-arc assemblage; (3) E-MOR basalts; (4) oceanic island-like basalt. Each type is characterized by its petrography, concentration of major, LILE, REE, and HFSE elements, and trace element ratios. Detailed petrographic and geochemical characteristics of rocks are given in the previous work [26]. For isotopic characterization, we selected samples from each rock group (Table 1).

Table 1. Characteristics of samples from the Ulan-Sar'dag ophiolite mélange used in this study.

Group	Sample	Rock	Modal Mineral Assemblage		
			Primary	Accessory	Secondary
Group I Boninite	293–16	Basaltic-andesite	Relics of Diopside–augite, plagioclase	Apatite	Actinolite, chlorite, epidote, biotite, titanite
	307–17	Ol peridotite	Olivine, orthopyroxene	Chromite	Amphibole: ferro-hornblende–ferro-pargasite, serpentine, talc, chrom-magnetite, magnetite
	294–17	Gabbro	Diopside, plagioclase–bitownite	Ilmenite, apatite	Amphibole: actinolite–hornblende–pargasite–tschermakite, albite, scapolite, epidote
Group II Island-arc assemblage	22–19 EF	Basalt	Clinopyroxene–diopside, plagioclase–bitownite	Chromite, ilmenite, apatite	Amphibole: actinolite–magnesian-hornblende–pargasite–tschermakite, chlorite, albite, epidote, scapolite
	24/1–19 WF	Basaltic-andesite	Plagioclase–oligoclase	Ilmenite, Rutile, apatite, zircon	Amphibole: actinolite–magnesian-hornblende, albite, epidote, sericite, titanite
	19b–19	Andesite	Plagioclase: oligoclase–andesine–labrador, potassiumfeldspar, biotite, quartz	Monazite, apatite, ilmenite, zircon	Amphibole: magnesian hornblende, albite, chlorite, garnet—almandine–spessartine, epidote, scapolite, muscovite, titanite
	35–18				
	310–16				
	47–19				
314–16					
Group III E-MORB	313–16	Basalt	Relics of diopside–augite, plagioclase: labrador–bitownite	Ilmenite, apatite	Amphibole: actinolite–vagnesian-hornblende–pargasite–tschermakite, chlorite, talc, albite–oligoclase, biotite, sericite
	93–17	Trachybasalt	Hornblende, albite, epidote, biotite	Ilmenite, apatite	Amphibole: magnesian-ferro-hornblende, biotite, albite, epidote, garnet, sericite, titanite
	18–19	Peridotite	Relics of clinopyroxene–diopside–augite, plagioclase–labradorite	Ilmenite, apatite, zircon	Actinolite, chlorite, albite–oligoclase, biotite, epidote, titanite, new-formed zircon
Group IV OIB	17–19	Melano gabbro	Relics of clinopyroxene–diopside–augite	Ilmenite, apatite, zircon	Amphibole: ferro hornblende–ferro pargasite, albite–oligoclase, biotite, epidote, titanite, new-formed zircon
	7a–19	Gabbro	Relics of clinopyroxene–diopside–augite and plagioclase–labradorite	Ilmenite, apatite, zircon	Amphibole: actinolite–ferro-hornblende, albite–oligoclase, biotite, epidote, titanite, new-formed zircon
	14–19				
	3–19	Monzo-gabbro	Clinopyroxene–diopside–augite, plagioclase–labradorite, potassium feldspar, biotite	Ilmenite, baddeleyite, apatite, zircon	Amphibole: ferro-hornblende–ferro-edenite–ferro-pargasite, plagioclase: albite–oligoclase, Epidote, titanite, new-formed zircon
	19a–19				

Abbreviations: Ol—olivine, Hyp—hypersthene, Di—diopside, Pl—plagioclase, Or—orthoclase, Npn—nepheline, Qz—quartz, Ap—apatite, Zrn—zircon, Chr—chromite, Mag—magnetite, Ilm—ilmenite, Ttn—titanite.

3.2. $^{40}\text{Ar}/^{39}\text{Ar}$ Isotope Analytical Method

The $^{40}\text{Ar}/^{39}\text{Ar}$ dating was carried out at the Analytical Center for Multi-Elemental and Isotope Research (VS Sobolev Institute of Geology and Mineralogy, Novosibirsk, Russia). The $^{40}\text{Ar}/^{39}\text{Ar}$ dating of a ground fraction of the whole-rock sample VSK-17-19 was carried out using the step-heating technique [38]. The samples were irradiated in the nuclear BWR reactor at the Tomsk Polytechnic University. A standard biotite sample MSA-11 (OSO No. 129-88) with an age of 311.0 ± 1.5 Ma, validated against international standard samples Bern-4M (muscovite) and LP-6 (biotite), was used as the fluence monitor.

The age of the Bern 4M and LP-6 were assumed to be 18.51 and 128.1 Ma, respectively [39]. The Ar isotopic composition in the irradiated samples was measured using a Noble Gas 5400 mass-spectrometer [38] Noble Gas 5400 (Micromass, United Kingdom, Manchester) mass-spectrometer S.N. SV022). The separation of gas fractions and the isotopic analysis of the argon in them was carried out in a temperature range from 500 to 1200 °C using a quartz furnace with external heating. The raw data were corrected for procedural blank contributions, mass discrimination by analysis of atmospheric Ar, de-cay of radioactive ^{37}Ar and ^{39}Ar isotopes produced by irradiation, and interferences of ^{36}Ar , ^{39}Ar , and ^{40}Ar produced from ^{40}Ca , ^{42}Ca , and ^{40}K , respectively. When correcting for isotopic mass fractionation, a value of $^{40}\text{Ar}/^{36}\text{Ar}$ in atmospheric argon was used equal to 298.6 [40]. For correction, the following coefficients were used: $(^{39}\text{Ar}/^{37}\text{Ar})_{\text{Ca}} = 0.001279 \pm 0.000061$, $(^{36}\text{Ar}/^{37}\text{Ar})_{\text{Ca}} = 0.000613 \pm 0.000084$, $(^{40}\text{Ar}/^{39}\text{Ar})_{\text{K}} = 0.0191 \pm 0.0018$. The amount of ^{40}Ar , ^{39}Ar , ^{38}Ar , ^{37}Ar , ^{36}Ar in the blank was normally about 3×10^{-10} , 2×10^{-12} , 2×10^{-11} , 1×10^{-12} , 9×10^{-12} cm³ STP, correspondingly. The errors in individual measurements for each of the steps in the spectrum are given taking into account the error, including both the analytical error and the error in determining the decay constant K. The isotopic ratio of $^{40}\text{Ar}/^{36}\text{Ar}$ characterizing instrument fractionation in a standard portion of air argon for the measurement period was 298 ± 2 . The plateau ages were calculated using the Isoplate 3.0 program (the program was created in 2006 by K.R. Ludwig at the Berkeley Geochronological Center, San Francisco, USA) if 60% or more of the ^{39}Ar was released in three or more contiguous steps, and the apparent ages agree to within 3σ of the integrated age of the plateau segment.

3.3. Sm-Nd Isotope Analytical Method

The whole-rock isotope research was carried out in the Collective Use Centre of the Kola Science Centre RAS (Apatity, Russia). In order to define concentrations of samarium and neodymium, the sample was mixed with a compound tracer $^{149}\text{Sm}/^{150}\text{Nd}$ prior to dissolution. It was then diluted with a mixture of HF + HNO₃ (or + HClO₄) in Teflon sample bottles at a temperature of 100 °C until complete dissolution. Further extraction of Sm and Nd was carried out using standard procedures with two-stage ion exchange and extraction-chromatographic separation using ion-exchange tar «Dowex» 50 × 8 in chromatographic columns employing 2.3 N and 4.5 N HCl as an eluent. The separated Sm and Nd fractions were transferred into nitrate form, whereupon the samples (preparations) were ready for mass-spectrometric analysis. The isotope Nd composition and Sm and Nd contents were measured on a 7-channel solid-phase mass-spectrometer (Finnigan MAT-262 (RPQ), “Thermo Fisher Scientific”, Waltham, MA, USA), in a static double-band mode, using Ta + Re filaments. A mean value of $^{143}\text{Nd}/^{144}\text{Nd}$ ratio in a JNd_i-1 standard was 0.512081 ± 13 (N = 11) in the test period. The error in $^{147}\text{Sm}/^{144}\text{Nd}$ ratios was 0.3% (2σ), which is a mean value for 7 measurements in a BCR-2 standard [41]. The blank intralaboratory contamination was 0.3 ng for Nd and 0.06 ng for Sm. The accuracy of estimation of Sm and Nd contents was $\pm 0.5\%$. Isotope ratios were normalized per $^{146}\text{Nd}/^{144}\text{Nd} = 0.7219$, and then recalculated for $^{143}\text{Nd}/^{144}\text{Nd}$ in JNd_i-1 = 0.512115 [42]. Values of $\epsilon_{\text{Nd}}(\text{T})$ and $T_{(\text{DM})}$ model ages were estimated using present-day values of CHUR after [43] at ($^{143}\text{Nd}/^{144}\text{Nd} = 0.512630$, $^{147}\text{Sm}/^{144}\text{Nd} = 0.1960$) and DM after [43] ($^{143}\text{Nd}/^{144}\text{Nd} = 0.513151$, $^{147}\text{Sm}/^{144}\text{Nd} = 0.21$).

3.4. Rb-Sr Isotope Analytical Method

The whole-rock isotope research was carried out in the Collective Use Centre of the Kola Science Centre RAS (Apatity, Russia). Distilled acids HCl, HF, HNO₃, and H₂O (distillate) were used to decompose samples. Then, the produced solution was divided into two aliquots to estimate the isotope composition and contents of Rb and Sr. The latter were estimated by isotope dissolution using an $^{85}\text{Rb}/^{84}\text{Sr}$ mixed tracer. Rb and Sr were extracted by elution chromatography on Dowex resin 50 × 8 (200–400 mesh) and 1.5 N and 2.3 N of HCl were used as eluates. The amount of resin in the used columns was ~ 7 cm³ and ~ 4 cm³. Extracted Rb and Sr concentrates were evaporated until dry and then

treated with several drops of HNO₃. The isotope composition of Sr and contents of Rb and Sr were estimated on an MI-1201-T mass spectrometer MI-1201T “Electron”, Sumy, Ukraine in a double-band mode using Ta + Re filaments. Prepared samples were placed onto the bands in a nitric form. The isotope composition of Sr in all of the measured samples was normalized per 0.710248 [44]. Errors in the estimation of the Sr isotope composition (95% confidence interval) were not higher than 0.04%; errors in the estimation of Rb–Sr ratios were 1.5%. The blank intralaboratory contamination in Rb and Sr was 2.5 ng and 1.2 ng, respectively. Correction of mass fractionation for Sr isotopic ratios was based on an ⁸⁸Sr/⁸⁶Sr value of 8.37521 using a power law.

4. Results

4.1. ⁴⁰Ar/³⁹Ar dating of the Mafic Dike

In order to constrain the minimum age of the Ulan-Sar’dag ophiolite mélange, a whole rock sample (VSK-17-19) was taken from a gabbro–diabase dike by cutting it for ⁴⁰Ar/³⁹Ar step-heating dating. The dating was performed by ⁴⁰Ar/³⁹Ar by step heating. The obtained age and Ca/K spectra of the sample are shown in Figure 6. In the age spectrum, a conditioned plateau was distinguished, characterized by 63% of the cumulative ³⁹Ar and a weighted mean plateau age (WMPA) value of 799 ± 11 Ma. Among the minerals that make up the dike rock, amphibole was the main potassium-containing mineral, with a minimum amount of biotite. Analyzing the nature of radiogenic argon release during step-heating, it can be noted that minimal amounts were released at low–medium temperatures (600–700 °C), at which biotite decomposition usually occurs in a vacuum. Most of the radiogenic argon is released at high temperatures (930–1100 °C), at which the crystal lattice of the amphibole is destroyed. Thus, it is logical to assume that the plateau observed in the age spectrum corresponded to the closure of the amphibole K–Ar isotope system. Considering that the introduction of dikes took place in shallow conditions and was accompanied by their rapid cooling, the dating obtained by the plateau method corresponded to the age of formation of the mafic dike. The ⁴⁰Ar/³⁹Ar weighted mean plateau age of 799 ± 11 Ma constrains the minimum age of the ophiolite mélange in the region, implying that all accretion ended in the early Neoproterozoic (late Tonian).

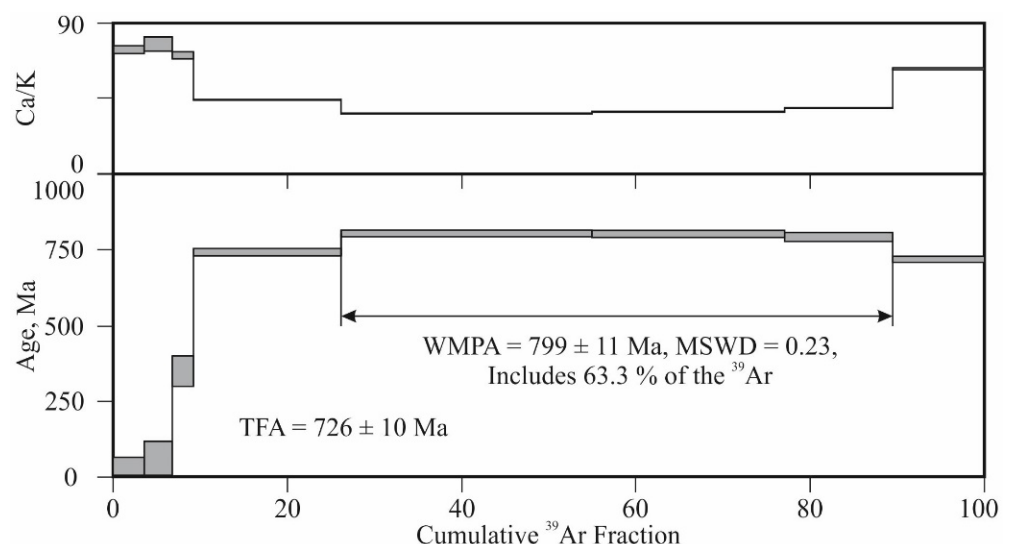


Figure 6. ⁴⁰Ar/³⁹Ar Ages and Ca/K Spectra of whole rock sample of mafic dike (VSK-17-19).

4.2. Geochemical Features and Nd–Sr Isotopes

The main and rare chemical composition of the studied rocks is presented in Table S1. A detailed geochemical characteristic of the magmatic rocks of the Ulan-Sar’dag ophiolite mélange is given in a previous study [26]. According to a previous study, the magmatic rocks belong to the following geochemical types (Figure 7): (1) ensimatic island-

arc boninites; (2) island-arc assemblage; (3) tholeiitic basalts of mid-ocean ridges; and (4) oceanic island-like basalts. The main and rare element chemical composition of the studied rocks is given in Table S1. Further, we present the isotopic characteristics for each group of rocks. Sixteen whole-rock samples were analyzed for Sr and Nd isotopic compositions. The results are given in Table S2 and plotted in Figure 8. For all samples, except for the mafic dikes, the $\epsilon_{Nd}(T)$ and $I_{Sr}(T)$ ratio was calculated to the date 833 Ma, and for the mafic dikes—799 Ma.

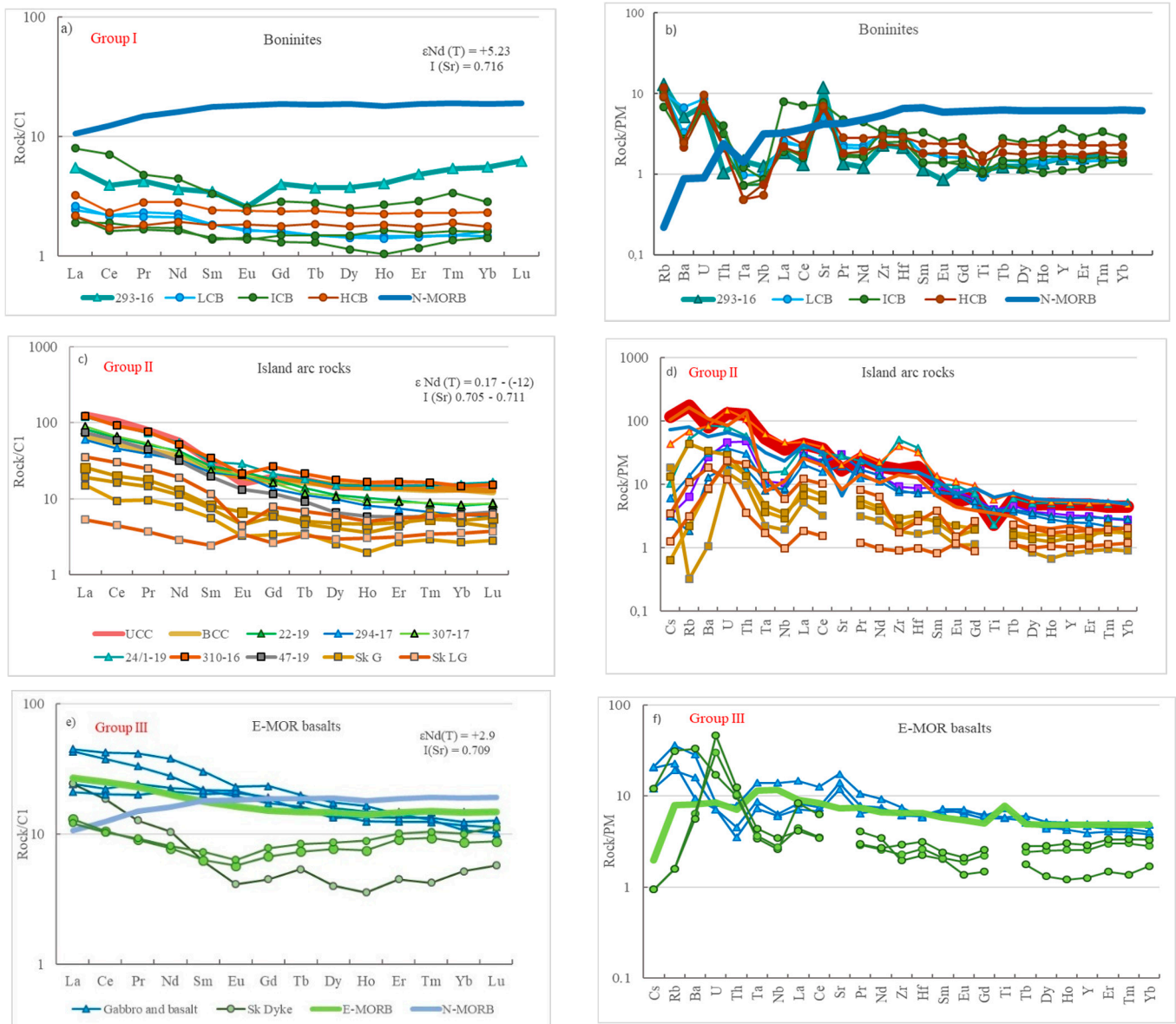


Figure 7. Cont.

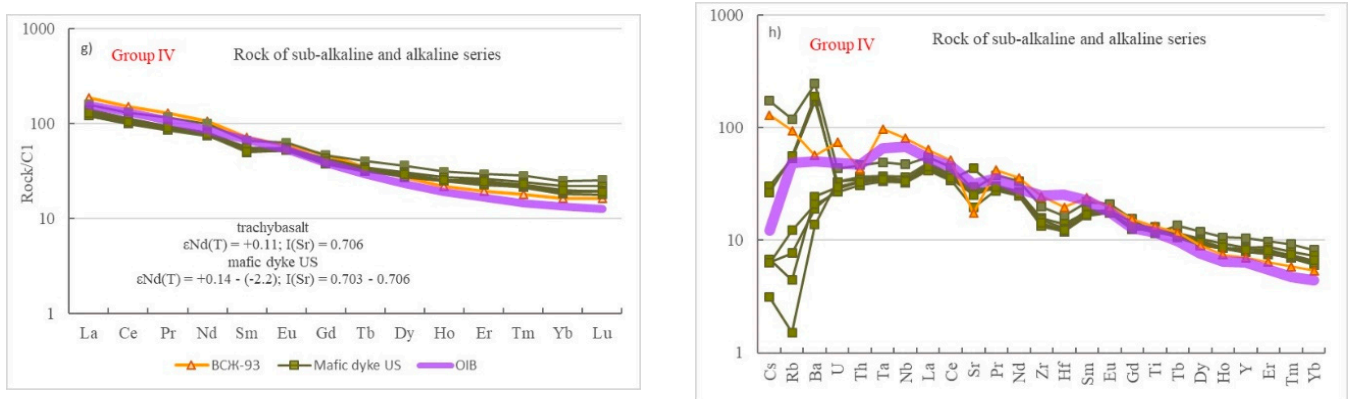


Figure 7. C1 chondrite normalized REE (rare earth elements) patterns and primitive mantle normalized trace element spidergram diagram for magmatic rocks of the Ulan-Sar'dag massif data from published data [26]; normalizing values are from [45]: (a,b) Group I—boninite USM and literature data [46]: Low calcium (LCB), medium calcium (ICB), high calcium (HCB) boninites; (c,d) group II— island-arc assemblage, Sk—Dunzhugur ophiolite massif, G—gabbro, LG—leyko gabbro, literature data [29]; (e,f) group III geochemical type—E-MORB basalts, Sk—Dunzhugur ophiolite massif, mafic dike literature data [29]; (g,h) group IV—OIB-like type geochemical group.

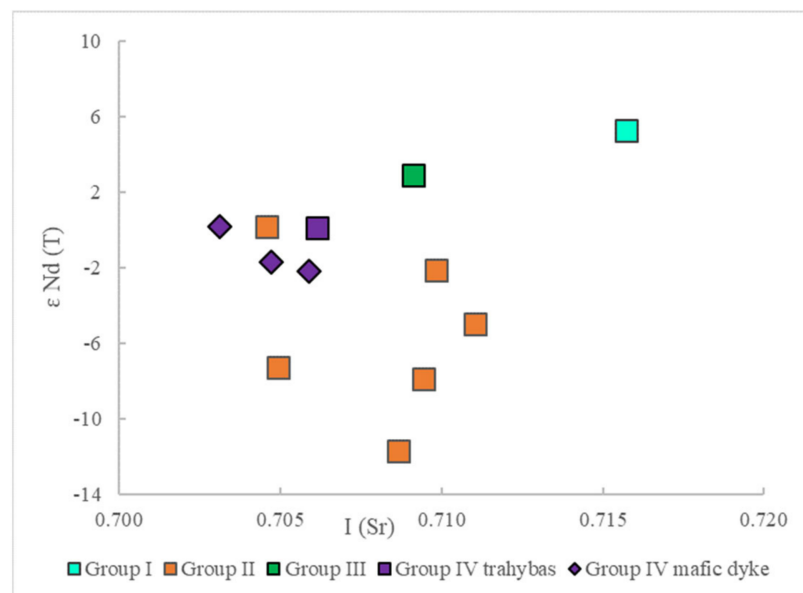


Figure 8. Ratios $I_{Sr}(T) - \epsilon_{Nd}(T)$. For all samples, except for the mafic dikes, $\epsilon_{Nd}(T)$ and the $I_{Sr}(T)$ ratio was calculated to the date 833 Ma, and for the mafic dikes -799 Ma.

The current ratios for the depleted mantle and CHUR were used to calculate $\epsilon_{Nd}(T)$ and T (DM) [43]. The first geochemical type—ensimatic island-arc boninites $(La/Sm)_n = 1.6$; $(Th/La)_{PM} = 0.5$; $^{147}Sm/^{144}Nd = 0.18$; $\epsilon_{Nd}(T) = (+5.23)$, model age T (DM) 1.4 Ga; $I_{Sr}(T)$ was high and was 0.715. The second geochemical type— island-arc assemblage had elevated values $(La/Sm)_n = 2.8-4$; $(Th/La)_{PM} = 1.4-5$; crustal values of $^{147}Sm/^{144}Nd = 0.10-0.12$, and only in the gabbro sample was this value 0.15. Rocks showed a wide range of $\epsilon_{Nd}(T)$, the values of which varied from $(+0.17)$ to (-12) ; T (DM) = 1.5–2.3 Ga. In the cumulative gabbro T (DM) was 2.0–2.2Ga, $\epsilon_{Nd}(T) = (-7.3)-(-2)$, $I_{Sr}(T) = 0.705-0.709$. In the basalt, andesi-basalt, andesite T (DM) varied 1.5–2.3Ga, $\epsilon_{Nd}(T)$ varied $(0.17)-(-12)$, $I_{Sr}(T) = 0.704-0.711$. Basalt of the third E-MORB geochemical type had a low ratio $(La/Sm)_n = 1$, $(Th/La)_{PM} = 0.5$ and the following isotopic parameters: $^{147}Sm/^{144}Nd$ ratio had a mantle value of 0.17, T (DM) = 1.7 Ga, $\epsilon_{Nd}(T) = (+3)$, and high values of $I_{Sr}(T) = 0.709$. The fourth transi-

tional to oceanic islands (OIB-like) geochemical type had an elevated isotopic value of $^{147}\text{Sm}/^{144}\text{Nd} = 0.13$, but lower than in the second geochemical type. It had an $(\text{La}/\text{Sm})_n$ 2.3–2.7, $(\text{Th}/\text{La})_{\text{PM}} = 0.7\text{--}0.8$, isotopic ratios $^{147}\text{Sm}/^{144}\text{Nd} = 0.13$, for both trachybasalt and mafic dike. For trachybasalt, T (DM) = 1.6 Ga, ϵ_{Nd} (833 Ma) = +0.11; I_{Sr} (833 Ma) = 0.706. For the mafic dike, T (DM) = 1.6–1.8 Ga, ϵ_{Nd} (799) (+0.14) to (−2); I_{Sr} (799) = 0.703–0.706.

5. Discussion

Based on the isotope geochemistry data, four geochemical types of rocks were distinguished: (1)—boninites, (2)—island-arc assemblage, (3)—EMOR basalts, (4) transitional to basalts of oceanic islands (OIB-like) [26] in the magmatic rocks of the Ulan-Sar'dag massif. According to the study of $^{147}\text{Sm}/^{144}\text{Nd}$ and $^{87}\text{Rb}/^{86}\text{Sr}$ isotopic systems, igneous rocks of the Ulan-Sar'dag massif are characterized by a significant dispersion of the values of isotopic parameters. The values of $^{147}\text{Sm}/^{144}\text{Nd}$ varied from mantle (0.18) [47,48] to crustal (0.10–0.13) [49] values, and ϵ_{Nd} (T)—from +0.17 to −12 (Table S2). Most of the rocks of the Ulan-Sar'dag massif had crustal values of $^{87}\text{Sr}/^{86}\text{Sr}$ (Table S2) and I_{Sr} (T) calculated to the date 833 Ma, except a few samples (gabbro, basalt, andesite) and samples from the mafic dike with mantle (but elevated) values, variations I_{Sr} (T) from 0.703 to 0.705 (Table S2), for most samples these values were 0.708–0.715. The ratio of ϵ_{Nd} (T)– I_{Sr} (T) did not correspond to the mantle sequence [49] (Figure 8). The model age determined from the Re-Os isotopy of mantle peridotites of the Ulan-Sar'dag massif was 1.38–2.38 Ga [31].

5.1. Constraints on Mantle Source

High-magnesium basaltic–andesite of the first geochemical type (boninite) has an REE distribution corresponding to boninites (Figure 7a,b), with low Ta/Yb, Th/Yb, $(\text{La}/\text{Sm})_n$ ratios close to N-MOR values, high Cr content > 500 ppm, $(\text{Th}/\text{La})_{\text{PM}} < 1$ [26]. Low REE concentrations and negative anomalies of HFSE (Nb, Ta, Ti) are typical for boninites [46]. In the discrimination diagrams, high-magnesium basaltic–andesite lies in the field of island-arc rocks and boninites [26]. Isotopic geochemical characteristics of the boninite: mantle value $^{147}\text{Sm}/^{144}\text{Nd}$ and positive value ϵ_{Nd} (T) = +5.23 (Figure 8, Table S2) confirm formation from a depleted mantle source with a long prehistory for this group of rocks. Model age T (DM) 1.4 Ga can be accepted as the age of the mantle source and possible as the forming age of an ensimatic island arc. Adjacent age was obtained for plagiogranites of the Dunzhugur ophiolite massif—1020 Ma and 1035 Ma—for Ilchir gabbro [20,33]. The $^{87}\text{Sr}/^{86}\text{Sr}$ values in the boninite were very high; both measured (0.717) and calculated to the date 833 Ma I_{Sr} (T) = 0.7157 and are comparable to the values in seawater, shales, gneiss [49–51]. The values $^{87}\text{Sr}/^{86}\text{Sr}$ in seawater NP, vary from 0.705 to 0.709 range [52]. The values $^{87}\text{Sr}/^{86}\text{Sr}$ in protoplatform carbonate sediments—dolomites of Irkut suite, range from 0.705 to 0.709 [53]. The value of $^{87}\text{Sr}/^{86}\text{Sr}$ in the boninite of the USM was close to $^{87}\text{Sr}/^{86}\text{Sr}$ in boninites from the Ospa–Kitoi and Dunzhugur massifs with $^{87}\text{Sr}/^{86}\text{Sr} = 0.713$ [32].

Gabbros, basaltic–andesite, andesites, dacites, and rhyolites of the second geochemical type have a slightly pronounced negative slope in the REE pattern (Figure 7c,d) and the distributions of REE, HFSE, and LILE, which fully corresponded to the distributions of the island-arc rocks. All rocks from this group had a negative anomaly for Ta, Nb, and Ti. In several samples, positive anomalies in Sr, Ba, Rb, and Zr were presented. The second group had a wide spectrum of island-arc geochemical affinities [26]. High Cr content > 800–500 ppm was established in the rocks of mafic composition. In andesites, the Cr content was much lower. Relationships Sr/Y , $(\text{Th}/\text{La})_{\text{PM}}$, which reflects the involvement of a subduction (crustal) component in the melt [54], varied from 5 to 47. It is supposed that there was no subduction component at $\text{Sr}/\text{Y} < 25$ (Table S1). Relation $(\text{Th}/\text{La})_{\text{PM}} > 1$ had values 1.4–5 (Table S1), except one peridotite sample. The rocks of the second group were characterized by an increased content of $\text{Th}/\text{Yb} = 2\text{--}4$ (Table S1), which is typical for modern subduction basalts [55]. Rocks of the second geochemical group had signs of participation of a crustal component in the magmatic source. The inverse relationship between $(\text{La}/\text{Sm})_{\text{PM}}\text{--}(\text{Nb}/\text{La})_{\text{PM}}$ (Figure 9), as for $(\text{Th}/\text{La})_{\text{PM}} > 1$, testified in favor of the

enrichment of the mantle source due to the subduction of metaterrigenous rocks (crustal material). Participation of the crustal material in the magmatic source has also been confirmed by Sm-Nd data of NP terrigenous rocks [56] and granite gneisses of the Gargan block (unpublished data by Turkina). For almost all samples from the second group, crustal values of $^{147}\text{Sm}/^{144}\text{Nd}$ of 0.10–0.12 were observed, and only in the gabbro sample, this value was 0.15. Model age T (DM) varied 1.5–2.3 Ga. This group was characterized by negative $\varepsilon_{\text{Nd}}(T)$ and high crustal values ($^{87}\text{Sr}/^{86}\text{Sr}$) and $I_{\text{Sr}}(T)$ having a large spread (Figure 8). The effect of the mature continental crust on the geochemical and isotopic compositions is established in many ophiolitic complexes in orogenic belts and magmatic rocks in igneous provinces [57,58], the Altai–Sayan region [59], Central Asian Fold Belt [60,61].

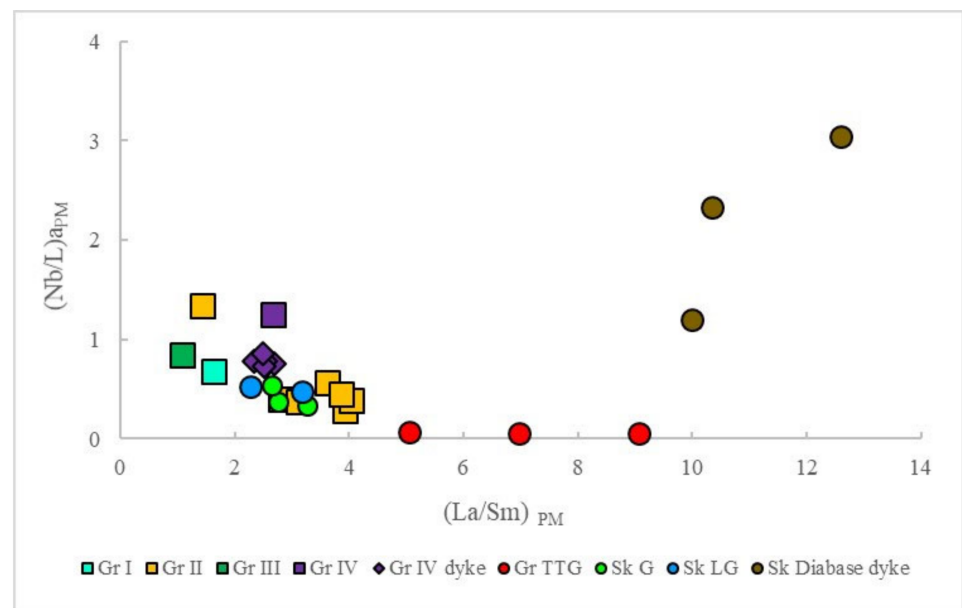


Figure 9. $(\text{La}/\text{Sm})_{\text{PM}}-(\text{Nb}/\text{La})_{\text{PM}}$ relations in the magmatic rocks of the different geochemical types (Gr I, II, III, IV) of the Ulan-Sar ‘dag massif, Dunzhugur massif (Sk): G—gabbro, LG—leyko–gabbro, diabase dike [29]; TTG complex of the Gargan block (Gr TTG) (Turkina unpublished data).

At the mixing of two magmatic sources and with crustal component participation, a negative correlation between $(\text{La}/\text{Sm})-\varepsilon_{\text{Nd}}(T)$ was established (Figure 10) [62]. Magmatic rocks of the second group have lain in the area of the mixing line of the two magmatic sources in the diagram $\varepsilon_{\text{Nd}}(T)-(\text{La}/\text{Sm})$ (Figure 10). Boninite was used as the last member, which is supposed to have a depleted mantle source. In addition, granite gneisses TTG with a low ε_{Nd} (833 Ma) = -23 value (unpublished data by Turkina O.M.), which provides a decline in the $\varepsilon_{\text{Nd}}(T)$ value for magmatic rocks at the low contribution of sediment matter was used. The contribution of various sources to the formation of igneous rocks was calculated using the binary mixing model [63]. The proportion of crustal components for the second group of rocks varied from 14 to 45% (Figure 11).

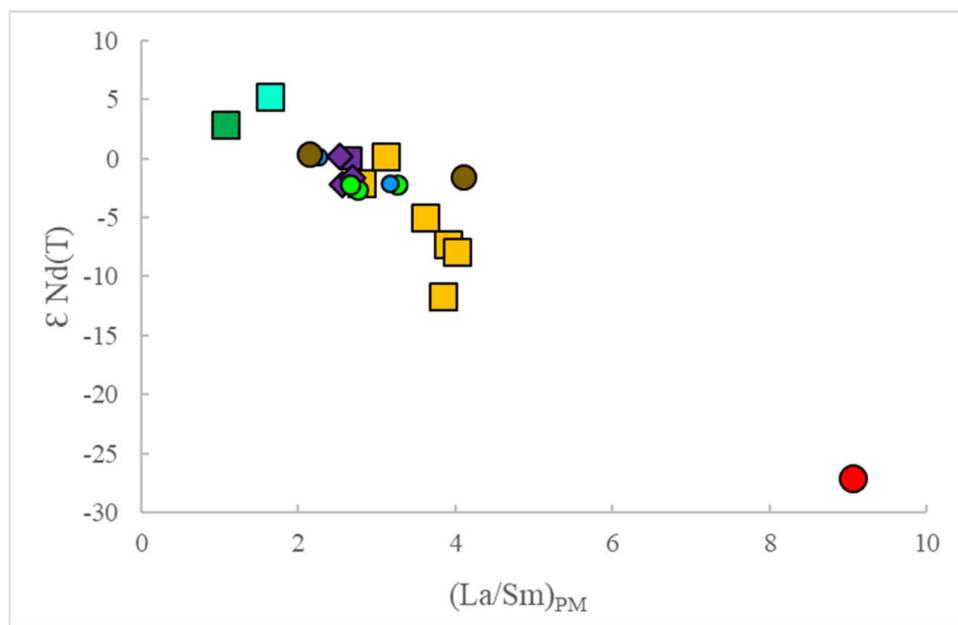


Figure 10. (La/Sm)_{PM}–εNd(T) relations in the magmatic rocks of the Ulan-Sar’dag massif (Group: I, II, III, IV), εNd (T) calculated at the date 833 Ma and mafic dike at the date 799 Ma; Dunzhugur massif (Sk): G—gabbro, LG—leyko–gabbro [29]; TTG complex of the Gargan block (Gr TTG) (Turkina unpublished data). The symbols are identical to Figure 9.

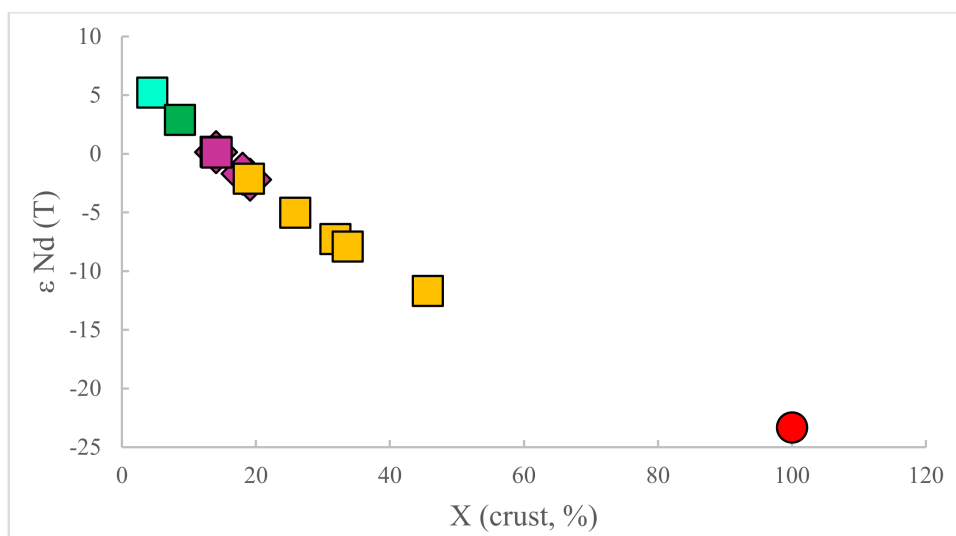


Figure 11. Diagram ε_{Nd}—contribution of Archean crust X (crust, %), demonstrating the contribution of different sources in the magma generation area. Archean crust contribution was calculated with two components of the mixing equation $X_m = 100 \times (\epsilon_1 - \epsilon_{mx}) \times Nd_1 / \epsilon_{mx} \times (Nd_2 - Nd_1) - (\epsilon_2 Nd_2 - \epsilon_1 Nd_1)$ [62], ε₁–ε_{Nd}(T) TTG Gargan block = (–23), Nd₁—concentration Nd in the TTG Gargan block = 22 ppm (unpublished data by Turkina O.M.), ε₂–ε_{Nd}(T) in the boninite of the Ulan-Sar’dag massif = +5, Nd₂—concentration Nd in the boninite = 2.92 ppm (this work); ε_{mx} —measured ε_{Nd}(T); X_m (%)—mantle component.

The high values of $^{87}\text{Sr}/^{86}\text{Sr}$ in all samples of the second group (gabbro, andesites), except for basalt and mafic dike, were comparable with such values in seawater, shales, gneiss. On the one hand, the $^{87}\text{Rb}/^{86}\text{Sr}$ isotopic system was more susceptible to the influence of metamorphogenic processes, and the safety of the system may be disturbed. On the other hand, the wide range and high values of $^{87}\text{Sr}/^{86}\text{Sr}$ may reflect the contribution of several sources: altered oceanic crust, terrigenous sediments of oceanic crust, mantle wedge above the subducting plate, sialic rocks of continental crust, or volcanic strata bases in island arcs [51,64,65]. During the ascent, the parental magmas could interact with rocks of the continental crust and sediments of the subducting slab. In the diagrams, $^{87}\text{Sr}/^{86}\text{Sr}$ – $^{143}\text{Nd}/^{144}\text{Nd}$, ϵNd_0 – $^{87}\text{Sr}/^{86}\text{Sr}$ (Figures 12 and 13), almost all samples fell into the field of continental crust, except for one sample, Nd–Sr isotopic ratios of which reflect either the characteristics of a magmatic source or its isotopic system were influenced by a younger mafic dike. The basalt (eastern flank of the massif, near the area of the mafic dike occurrence) from the second geochemical group in the $^{87}\text{Sr}/^{86}\text{Sr}$ – $^{143}\text{Nd}/^{144}\text{Nd}$ diagram lies in the field of the EM I source (Figure 12). In diagram ϵNd_0 – $^{87}\text{Sr}/^{86}\text{Sr}$ (Figure 13), basalt lies on the mixing line of the Prevalent mantle, upper continental crust, and Pacific pelagic sediments. Positive values of $\epsilon\text{Nd}(T)$ in the basalt indicate a juvenile source of these rocks. The ϵNd in comparison with the value of $\epsilon\text{Nd}(833\text{ Ma})$ for DM = (+8.2), may indicate the participation of melts from enriched sources in the generation of these rocks, or the influence of the introduced mafic dike (the fourth geochemical group) on the isotopic system of the basalt. On the tectonic discrimination diagram, the rocks of the second group are plotted in the fields of a volcanic arc, island-arc tholeiite, calc-alkaline basalts, and continental arc [26]. According to geochemical and isotopic parameters, rocks of the second group were generated from an enriched magmatic source due to a subduction component. The source of the terrigenous–sedimentary material was most likely rocks of the Archean TTG complex of the Gargan block (Figure 11).

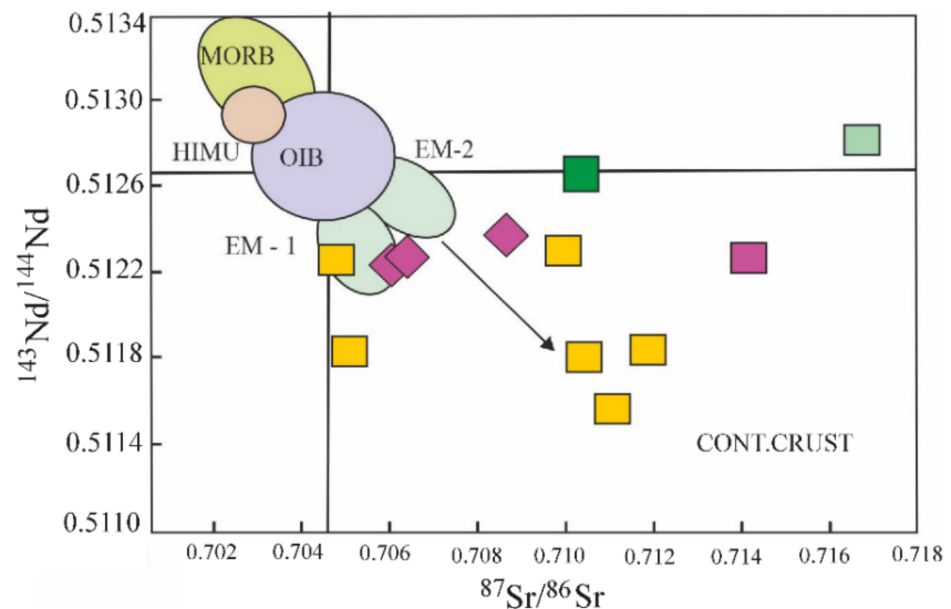


Figure 12. $^{87}\text{Sr}/^{86}\text{Sr}$ – $^{143}\text{Nd}/^{144}\text{Nd}$ relations in mantle sources and the magmatic rocks of the Ulan-Sar'dag massif.

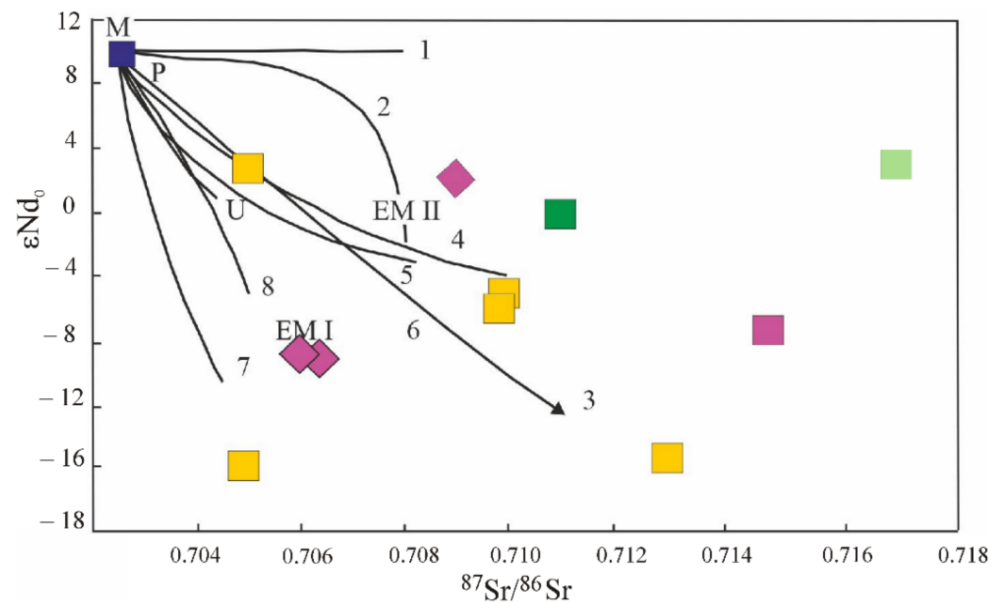


Figure 13. Sr-Nd isotopic mixing lines of magmas of type MORB ($\epsilon_{Nd}(T) = 10$, Nd = 7 ppm, $^{87}Sr/^{86}Sr = 0.7025$, Sr 130 ppm). Lines 1—modified oceanic basalts; 2—Phanerozoic marine carbonates; 3—average of upper continental crust ($\epsilon_{Nd}(T) = 10$, Nd = 7 ppm, $^{87}Sr/^{86}Sr = 0.7025$, Sr 130 ppm); 4—average of Pacific pelagic sediments ($\epsilon_{Nd}(T) = -4$, Nd = 20 ppm, $^{87}Sr/^{86}Sr = 0.710$, Sr 170 ppm) [66]; 5—pelagic sediments of the north part of Pacific ocean ($\epsilon_{Nd}(T) = -3$, Nd = 24 ppm, $^{87}Sr/^{86}Sr = 0.7083$, Sr 135 ppm by [67]; 6—lower crust ($\epsilon_{Nd}(T) = -10$, Nd = 30 ppm, $^{87}Sr/^{86}Sr = 0.710$, Sr 400 ppm by [68,69]; 7—lower crust ($\epsilon_{Nd}(T) = -10.4$, Nd = 32 ppm, $^{87}Sr/^{86}Sr = 0.7045$, Sr 370 ppm according to [64]; 8—Precambrian sedimentary dolomites ($\epsilon_{Nd}(T) = -5$, Nd = 2 ppm, $^{87}Sr/^{86}Sr = 0.705$, Sr 50 ppm). U—primitive undepleted mantle [49], EM1—enriched mantle 1, EM2—enriched mantle 2, P—Prevalent mantle [70,71].

The geochemical characteristics of the basalts and one gabbro sample from the third group of rocks corresponded to E-MOR basalts, except for LILE elements (Cs, Rb, Ba, and U) [26]. Sr/Y values < 25, $(Th/La)_{PM} < 1$, suggested the absence of a subduction component in the melt (Table S1), although elevated concentrations of Rb, Ba, Sr (Table S1) indicated the enrichment of the mantle source with incoherent elements. In general, the rocks had hybrid characteristics of N-MOR, E-MOR basalts. Basalt from this group had mantle values of $^{147}Sm/^{144}Nd = 0.17$, unlike basalt from the second geochemical group. The value of $\epsilon_{Nd}(T)$ was positive (+3) (Table S2), which may indicate the origin of this group of rocks from a poorly enriched mantle source. The positive $\epsilon_{Nd}(T)$ implied an injection of the upwelling asthenosphere into the arc segment, which would have provided a fertile mantle. A high value of $^{87}Sr/^{86}Sr = 0.710$, $I_{Sr}(T) = 0.709$, was recorded in basalt, which was comparable to the values in Proterozoic shales, gneiss. On the tectonic diagrams, rocks of this group fell into the fields of MOR and E-MOR basalts [26].

According to geochemical characteristics, the fourth geochemical type corresponded to ocean island-like basalt [26] (Figure 7g,h; Table S1). The rocks were enriched with both LREE and HREE, HFSE. The Sr/Y < 25, $(Th/La)_{PM} < 1$, had elevated concentrations of Ta, Th, Yb, which may indicate the involvement of asthenospheric melts [26,72–75]. According to $^{147}Sm/^{144}Nd$ systematics, the fourth group was close to the second group, having island-arc geochemical characteristics. The $^{147}Sm/^{144}Nd$ value had crustal values (0.13) in both trachybasalt and the mafic dike. The values of $\epsilon_{Nd}(T)$ for trachybasalt were close to chondrite (+0.11), for mafic dike, calculated to the date 799 Ma $\epsilon_{Nd}(T)$, and fit into a small range from close to chondrite to weakly negative values (+0.14)–(−2.2). The calculated model age for trachybasalt T(DM) was 1.5 Ga, for mafic dike, 1.5–1.8 Ga (Table S2). In the diagram $(La/Sm)_{PM} - \epsilon_{Nd}(T)$, the rocks of the third and fourth geochemical groups lie between boninite and island-arc assemblage (Figure 10). The values of $I_{Sr}(T)$ in the fourth

group had a mantle but elevated values of 0.703–0.706. Isotope ratios in the mafic dikes (the fourth geochemical group) in the diagrams, $^{87}\text{Sr}/^{86}\text{Sr}$ – $^{143}\text{Nd}/^{144}\text{Nd}$, ϵ_{Nd_0} – $^{87}\text{Sr}/^{86}\text{Sr}$ plotted in the field of the mantle source EM I are shown in Figures 12 and 13. Isotope geochemical characteristics of the third and fourth groups are probably likely indicative of a mixture of island-arc melts with asthenospheric melts. Geodynamic processes could be associated with the rollback of the subducting oceanic lithosphere, slab breakoff, upwelling asthenosphere, and decompression melting. It would produce E-MORB and OIB-like magma with high $^{87}\text{Sr}/^{86}\text{Sr}$ and low $^{143}\text{Nd}/^{144}\text{Nd}$ values [73–75]. Further, these processes could lead to an extension of the Dunzhugur island arc that can be attributed to intra-arc rifting and subsequent formation the Shishkhid back-arc basin [4].

5.2. Comparison Isotope Data of Ulan-Sar'dag Massif with Ospa–Kitoi and Dunzhugur Massifs

Comparing the isotopic and geochemical characteristics of the ophiolite rocks and associated island-arc assemblage of the Ulan-Sar'dag massif and the mafic rocks closest to them in geochemical characteristics (island-arc type) from the ophiolite association of the Dunzhugur and Ospa–Kitoi ophiolite massifs, it can be seen that the gabbro of the Dunzhugur massif had increased values $(\text{La}/\text{Sm})_n$ from 1.7 to 4, $(\text{Th}/\text{La})_n > 1$ (1.2–3). It was similar to the rocks in the second group of the Ulan-Sar'dag massif array, indicating a crustal component contribution in the result of subduction settings. The calculated $\epsilon_{\text{Nd}}(T)$ for the age accepted for the Dunzhugur island arc of 1020 Ma had a small spread of values, fitting into the range (+1)–(–1) and, accordingly, a smaller range of values of T (DM) 1.7–2.2 Ga, which also confirmed the contribution of the crustal component (Figures 9 and 10). The geochemical characteristics of the Dunzhugur massif diabase dikes were similar to the geochemical characteristics of basalts group III. They were characterized by low, but positive values of $\epsilon_{\text{Nd}}(T)$. $^{147}\text{Sm}/^{144}\text{Nd}$ ratios had both crustal (0.12), and mantle (0.17) values [29]. At the same time, the mafic dike of the USM, in contrast to the diabase dikes of the Dunzhugur massif, contained high concentrations of REE, HFSE, Th.

Cumulative and volcanic rocks of the Ospa–Kitoi massif had an $\epsilon_{\text{Nd}}(1020)$ from +4.3 to –2 [32] comparable to the isotopic parameters of magmatic rocks of the USM but differed from them in geochemical affinities.

5.3. Isotopic Evidence of Crust–Mantle Interaction

Isotopic data obtained for various complexes of the Eastern Sayan of the Central Asian Folded Belt [60] (Table 2) indicated a significant contribution of ancient crustal material to the genesis of the ophiolite and island-arc rocks of the Eastern Sayan, suggesting a model of mixing of the Neoproterozoic juvenile source and Archean crustal source (tonalite–trondhjemite gneisses of the Gargan block), which will give a wide range of $\epsilon_{\text{Nd}}(T)$ values from negative to positive values, depending on the proportion of crustal material.

Table 2. Isotope characteristics of the USM and other complexes East Sayan segment of the CAOB.

Geochemical Type/Rock	$[\Delta \text{Nb}]$	Age	$\epsilon_{\text{Nd}}(T)$	T (DM) Ga	Reference
Group I	–0.2	833 Ma (U–Pb)	+5.23	1.4	This work
Group II	(–1.27)–(+0.08)	833 Ma (U–Pb)	+0.17–(–11.7)	0.8–2.3	This work
Group III	(+0.1)–(+0.3)	833 Ma (U–Pb)	+3	1.6–3.4	This work
Group IV Trachybasalt Diabase dike	+0.2 +0.3	833 Ma (U–Pb) 799 Ma ($^{40}\text{Ar}/^{39}\text{Ar}$)	+0.11 +0.1–(–2.2)	1.5–1.8	This work
Dunzhugur ophiolite massif	No data	1020 Ma (U–Pb)	+1.5–(–1)	1.6–1.8	[29]
Ospa-Kitioi ophiolite massif	No data	1020 Ma (U–Pb) 1035 Ma (U–Pb)	(+4.3)–(–2)	No data	[32,33]

Table 2. Cont.

Geochemical Type/Rock	[Δ Nb]	Age	ENd(T)	T (DM) Ga	Reference
Shishkhid island arc complex with supra-subduction ophiolite	No data	850–800 Ma (U–Pb)	(+3.3)–(+6.9) (two samples yielded the values of 0.0)	No data	[4]
Sarkhoi continental arc complex	No data	782 Ma (U–Pb)	−0.6–(−9.2)	1.5–2.3	[60]
Oka accretionary prism (clastic sediments and felsic volcanic rocks)	No data	800 Ma (U–Pb) 775 Ma (U–Pb)	−0.5–(−9.1) −4.8–(−1.1)	1.5–2.3 1.5–1.9	[4,21,60,76]
Sumsunur tonalite sincollisional plutons	No data	785–811 Ma (U–Pb)	+13.2–(−12.3)	2.4–2.5	[4,54]
TTG Gargan block	No data	3100–2000 Ma (U–Pb)	(+1.3)–(−0.2)	2.9–3.0	Unpublished data by Turkina O.M., [77]

Δ Nb = Log (Nb/Y) + 1.74 – 1.92 × Log (Zr/Y) by [78].

A perfect example of contamination crustal matter and its influence on the isotopic characteristics of rocks formed from mantle sources is the Dovyren ultrabasite–basite stratified massif (quite well preserved) [65] which has an extensive range of values of I_{Sr} (T) 0.709–0.715. Isotopic characteristics for peridotites and basic rocks of the Dovyren massif [65] were $^{147}Sm/^{144}Nd$ 0.12; $^{144}Nd/^{143}Nd$ 0.511350–0.511704; ϵ_{Nd} (670 Ma) from −14 to −15; Sr 17–338 ppm, $^{87}Rb/^{86}Sr$ 0.02; I_{Sr} (T) 0.71–0.712. Isotopic characteristics for shales from the host frame of the Dovyren massif were $^{147}Sm/^{144}Nd$ 0.11–0.12; $^{144}Nd/^{143}Nd$ 0.5116–0.5118; ϵ_{Nd} (670 Ma) from −7 to −11; $^{87}Rb/^{86}Sr$ 0.5–2; I_{Sr} (T) 0.716–0.745; dolomites $^{147}Sm/^{144}Nd$ 0.143; $^{144}Nd/^{143}Nd$ 0.512633; I_{Sr} (T) 0.705. The reasons for crustal isotopic characteristics for $^{147}Sm/^{144}Nd$ and $^{87}Rb/^{86}Sr$ systems may be fluid exchange with host rocks during the post-crystallization process or disturbance of $^{87}Rb/^{86}Sr$ isotope system during metamorphism. According to the author [65], the change processes for the following reasons do not cause all variations of $^{87}Sr/^{86}Sr$: in peridotites, there is more than a 30-fold variation of Sr, but they show close I_{Sr} (T) values. If one supposes variations in $^{87}Sr/^{86}Sr$ ratios are the result of changes, then a hypothetical mechanism should provide a certain fluid–rock ratio. The concentration of Sr in the fluid is proportional to the concentration of Sr in the rock with which the fluid interacts [65].

5.4. The Stages of Magmatism of the Ulan-Sar'dag Massif

According to the isotope geochemical data of the Ulan-Sar'dag massif, we propose three stages of magmatism, reflecting the evolution of the arc magmatism and subduction zone in the studied segments of CAOB (Figure 14).

Stage I. In the Meso-Neoproterozoic, the intra-oceanic ensimatic island-arc system was formed. Boninite has positive ϵ_{Nd} (T) and is formed from a depleted mantle source. The high value of I_{Sr} (T) is due to the disturbance of the closure $^{87}Rb/^{86}Sr$ isotopic system: interaction with seawater and metamorphic processes.

Stage II. During the development of an ensialic island arc, boninite magmatism turned to calc-alkaline andesite magmatism at Neoproterozoic, which occurred with the involvement of subducted sediments both oceanic and terrigenous (Proterozoic gneiss of the Gargan block) to the magma generation chamber, which leads to a dispersion of isotopic parameters, negative values of ϵ_{Nd} (T), and the ancient of model ages, and high I_{Sr} (T).

Stage III. The subducting oceanic lithosphere had been proceeded by rollback, slab breakoff, upwelling asthenosphere, and decompression melting to produce E-MOR and OIB-like basites. Mixing asthenospheric melts with island-arc magmas can lead to enrichment of melts with radiogenic Nd and Sr and correspond to EM1 mantle source.

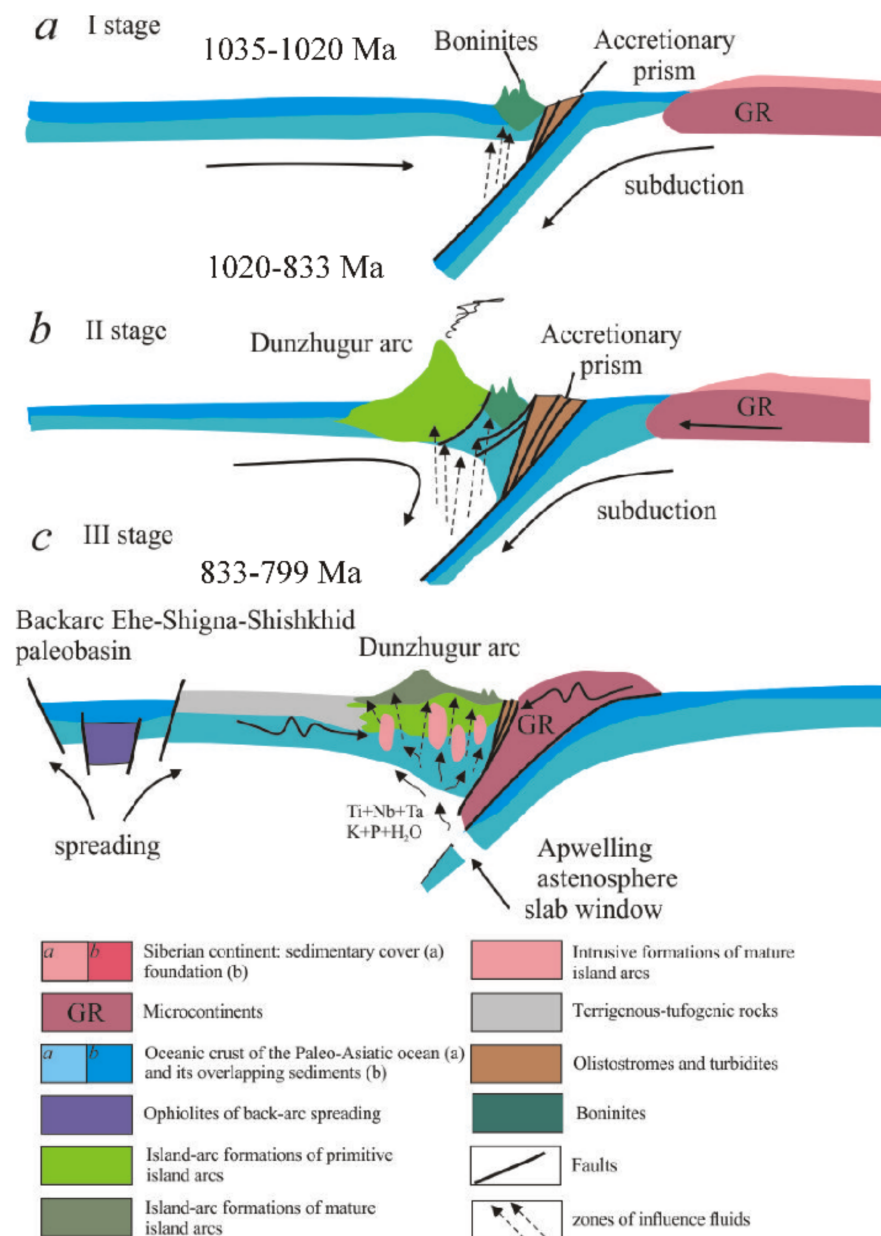


Figure 14. Simplified model of multistage magmatism at late Neoproterozoic (Tonian) time frame of a Pale-Asian Ocean segment. (a) I stage—ensimatic island-arc; (b) II stage—ensialic island arc; (c) III stage—slab breakoff, mixing asthenospheric melts with island-arc magmas.

The Ulan-Sar'dag Massif is a member of the Proterozoic ophiolite and island-arc systems in the CAO. They have subduction geochemical characteristics and were formed on the Neoproterozoic active continental margin of the Siberian paleocontinent. Proterozoic ophiolite and island-arc systems are associated with the evolution of the Paleo-Asian ocean in the period 1050–790 Ma. The island-arc assemblage of the Ulan-Sar'dag massif has geochemical characteristics of both ensimatic and ensialic island arcs. The stage of the initiation of ensimatic island arc magmatism in the Paleo-Asian ocean occurred in the time fence of 1050–790 Ma and is most widely developed in the Eastern Sayan, Northern and Eastern Baikal Lakeside, Mongolia [2–4,6,7,9,20,79,80]. The initiation of ensialic arc magmatism on the Neoproterozoic active margin occurred 830–780 Ma (Eastern Sayan, Central Transbaikalia, Mongolia) [21,56,60,77]. The formation of plumes associated with the melting of slabs plunging into the subduction zone and the participation of asthenospheric melts in island-arc magmatism occurred at the boundary of 820–770 Ma in almost all

Neoproterozoic island-arc systems with the formation of subalkaline–alkaline magmatic series [79,80]. The collisional granites formed at the 750 Ma boundary recorded collisional- orogenic events and accretion of island arcs at the Proterozoic stage [4,19].

6. Conclusions

1. The Ulan-Sar'dag massif consists of various structurally combined material blocks–ophiolite ultramafic–mafic rocks with podiform chromitites, cumulative gabbro, foliated serpentinites, island-arc assemblage, mafic dikes. Four isotope geochemical types of the magmatic rocks of the USM have been established.
2. The ophiolites of the Eastern Sayan belong to the supra subduction type. The first isotopic data on the magmatic rocks of the USM was obtained. Isotope geochemical characteristics of the magmatic rocks of the USM reflect the evolution of island arc magmatism and subduction zone. The boninite was formed from a depleted mantle source, and the island-arc assemblage was originated from an enriched mantle source which results from the subduction of terrigenous matter. The calculated proportion of the crustal component was from 14% to 45%. The source of the terrigenous material was most likely the rocks of the Archean TTG complex of the Gargan block. The E-MOR and OIB-like basalts and mafic dike were probably generated by mixing island-arc melts with asthenospheric melts produced from upwelling asthenosphere and decompression melting.
3. A whole-rock $^{40}\text{Ar}/^{39}\text{Ar}$ weighted mean plateau age of 799 ± 11 Ma constrains the minimum age of the ophiolite mélange in the region, implying that all accretion ended in the early Neoproterozoic (late Tonian).
4. The Ulan-Sar'dag Massif is a member of the Proterozoic ophiolite and island-arc systems in the CAO. They have subduction geochemical characteristics and were formed on the Neoproterozoic active continental margin of the Siberian paleocontinent. Proterozoic ophiolite and island-arc systems were associated with the evolution of the Paleo-Asian ocean in the period 1050–790 Ma. The island-arc assemblage of the Ulan-Sar'dag massif has geochemical characteristics of both ensimatic and ensialic island arcs. The stage of the initiation of ensimatic island arc magmatism in the Paleo-Asian ocean occurred in the time fence of 1050–790 Ma and is most widely developed in the Eastern Sayan, Northern and Eastern Baikal Lakeside, Mongolia. The initiation of ensialic arc magmatism on the Neoproterozoic active margin occurred 830–780 Ma (Eastern Sayan, Central Transbaikalia, Mongolia). The formation of plumes associated with the melting of slabs plunging into the subduction zone and the participation of asthenospheric melts in island-arc magmatism occurred at the boundary of 820–770 Ma in almost all Neoproterozoic island-arc systems with the formation of subalkaline enriched alkaline magmatic series. The collisional granites formed at the 750 Ma boundary recorded collisional- orogenic events and accretion of island arcs at the Proterozoic stage.

Supplementary Materials: The following supporting information can be downloaded at <https://www.mdpi.com/article/10.3390/min12010092/s1>, Table S1: Chemical composition of the magmatic rocks of the Ulan-Sar'dag ophiolite mélange used for isotope study, Table S2: The Nd-Sr isotope data of the magmatic rocks from the Ulan-Sar'dag ophiolite mélange.

Author Contributions: Conceptualization, O.K., E.A., P.S. and S.Z.; methodology, P.S. and A.T.; software, D.B.; validation, P.S., A.T. and S.Z.; formal analysis, O.K. and E.A.; investigation, O.K., E.A., and B.N.; resources, O.K. and B.N.; data curation, O.K.; writing—original draft preparation, O.K. and B.N.; writing—review and editing, O.K., P.S., A.T., E.A., D.B. and S.Z.; visualization, D.B. and B.N.; supervision, S.Z. and P.S.; project administration, O.K.; funding acquisition, O.K. All authors have read and agreed to the published version of the manuscript.

Funding: This research was funded by the Ministry of Science and Higher Education of the Russian Federation and the Russian Foundation for Basic Research, grants No. 19-05-00764a. Work was done on state assignment to IGM SB RAS.

Acknowledgments: The work was carried out at the Analytical Center for Multi-Elemental and Isotope Research, SB RAS (Novosibirsk, Russia) and in the Collective Use Centre of the Kola Science Centre RAS (Apatity, Russia). The authors are grateful to Semyon Kovalev for correcting the geological figures and to Daniil Yanov for their help in the English edition of the manuscript. The authors are grateful to Anatoliy Gibsher for providing the geodynamic scheme. The authors are grateful to the anonymous reviewers who essentially improved the manuscript.

Conflicts of Interest: The authors declare no conflict of interest.

References

1. Dobretsov, N.L. (Ed.) *Geology and Metamorphism of East Sayan*; Nauka Publ. House: Novosibirsk, Russia, 1988; p. 190. (In Russian)
2. Sengör, A.M.C.; Natal'in, B.A. Palaeotectonics of Asia: Fragments of a synthesis. In *The Tectonic Evolution of Asia*; Yin, A., Harrison, T.M., Eds.; Cambridge University Press: Cambridge, UK, 1996; pp. 486–640.
3. Torsvik, T.H.; Smethurst, M.A.; Meert, J.G.; Van der Voo, R.; McKerrow, W.S.; Brasier, M.D.; Sturt, B.A.; Walderhaug, H.J. Continental break-up and collision in the Neoproterozoic and Paleozoic—A tale of Baltica and Laurentia. *Earth Sci. Rev.* **1996**, *40*, 229–258. [[CrossRef](#)]
4. Kuzmichev, A.V. *The Central Asian Fold Belt. Geology, Evolution, Tectonics and Models*; Kröner, A., Ed.; Burntraeger Science Publisher: Studgard, Germany, 2015.
5. Dobretsov, N.L.; Buslov, M.M.; Vernikovskiy, V.A. Neoproterozoic to Early Ordovician evolution of the Paleo-Asian ocean: Implications to the break-up of Rodinia. *Gondwana Res.* **2003**, *6*, 143–159. [[CrossRef](#)]
6. Zhmodik, S.M.; Postnikov, A.A.; Buslov, M.M.; Mironov, A.G. Geodynamics of the Sayan-Baikal-Muya accretion-collision belt in the Neoproterozoic-early Paleozoic and regularities of the formation and localization of precious-metal mineralization. *Russ. Geol. Geophys.* **2006**, *1*, 183–198.
7. Windley, B.F.; Alexeiev, D.; Xiao, W.J.; Kröner, A.; Badarch, G. Tectonic models for accretion of the Central Asian Orogenic Belt. *J. Geol. Soc. Lond.* **2007**, *164*, 31–47. [[CrossRef](#)]
8. Dobretsov, N.L.; Konnikov, E.G.; Dobretsov, N.N. Precambrian ophiolitic belts of Southern Siberia (Russia) and their metallogeny. *Precambrian Res.* **1992**, *58*, 427–446. [[CrossRef](#)]
9. Sklyarov, E.V.; Gladkochub, D.P.; Mazukabzov, A.M.; Men'shagin, Y.V.; Konstantinov, K.M.; Watanabe, T. Dike swarms of southern flank of Siberian craton—Indicators of Rodinia supercontinent breakup. *Geotektonika* **2000**, *6*, 59–70.
10. Buslov, M.M.; Saphonova, I.Y.; Watanabe, T.; Obut, O.T.; Fujiwara, Y.; Iwata, K.; Semakov, N.N.; Sugai, Y.; Smirnova, L.V.; Kazansky, A.Y. Evolution of the Paleo-Asian ocean (Altai–Sayan region, Central Asia) and collision of possible Gondwana-derived terranes with the southern marginal part of the Siberian continent. *Geosci. J.* **2001**, *5*, 203–224. [[CrossRef](#)]
11. Meert, J.G.; Torsvik, T.H. The making and unmaking of a supercontinent: Rodinia revisited. *Tectonophysics* **2003**, *375*, 261–288. [[CrossRef](#)]
12. Yarmolyuk, V.V.; Kovalenko, V.I. Late Riphean breakup between Siberia and Laurentia: Evidence from intraplate magmatism. *Dokl. Earth Sci.* **2001**, *379*, 525–552.
13. Yarmolyuk, V.V.; Kovalenko, V.I.; Kozlovskiy, A.M.; Kudryashova, E.A.; Anisimova, I.V.; Sal'nikova, E.B.; Kovach, V.P.; Kozakov, I.K.; Kotov, A.B.; Plotkina, Y.V.; et al. Late Riphean alkali granites of the Zabhan microcontinent: Evidence for the timing of Rodinia breakup and formation of microcontinents in the Central Asian fold belt. *Dokl. Earth Sci.* **2008**, *420*, 583–588. [[CrossRef](#)]
14. Xiao, W.J.; Kusky, T.M. Geodynamic processes and metallogenesis of the Central Asian and related orogenic belts: Introduction. *Gondwana Res.* **2009**, *16*, 167–169. [[CrossRef](#)]
15. Xiao, W.J.; Huang, B.C.; Han, C.M.; Sun, S.; Li, J.L. A review of the western part of the Altai: A key to understanding the architecture of accretionary orogens. *Gondwana Res.* **2010**, *18*, 253–273. [[CrossRef](#)]
16. Aktanov, V.I.; Dorinna, N.A.; Posokhov, V.F.; Sklyarov, E.B.; Skopintsev, V.G. On the age and structure of the Gargan massif (south eastern Sayan) [abs.]. In Proceedings of the Conference on Structural Analyses of Crystalline Complexes, Irkutsk, Russia, 17–22 May 1992; Melnikov, A.I., Ed.; Institute of the Earth's Crust RAS: Irkutsk, Russia, 1992; pp. 89–90. (In Russian).
17. Dobretsov, N.L.; Buslov, M.M.; Safonova, I.Y.; Kokh, D.A. Fragments of oceanic islands in the Kurai and Katun' accretionary wedges of Gorny Altai. *Russ. Geol. Geophys.* **2004**, *45*, 1325–1348.
18. Letnikova, E.F.; Geletii, N.K.; Sklyarov, E.V. Lithological and Geochemical Features of Carbonate Rocks in the Sedimentary Cover of the Gargan Terrain, Southeastern East Sayan. *Gondwana Res.* **2001**, *4*, 680. [[CrossRef](#)]
19. Kuzmichev, A.B.; Bibikova, E.V.; Zhuravlev, D.Z. Neoproterozoic (~800 Ma) orogeny in the Tuva–Mongolia Massif (Siberia): Island arc–continent collision at the northeast Rodinia margin. *Precambrian Res.* **2001**, *110*, 109–126. [[CrossRef](#)]
20. Khain, E.V.; Bibikova, E.V.; Kröner, A.; Zhuravlev, D.Z.; Sklyarov, E.V.; Fedotova, A.A.; Kravchenko-Berezhnoy, I.R. The most ancient ophiolite of the Central Asian fold belt: U–Pb and Pb–Pb zircon ages for the Dunzhugur Complex, Eastern Sayan, Siberia, and geodynamic implications. *Earth Planet. Sci. Lett.* **2002**, *199*, 311–325. [[CrossRef](#)]
21. Kuzmichev, A.B.; Larionov, A.N. Neoproterozoic island arcs of East Sayan: Duration of magmatism (from U–Pb zircon dating of volcanic clastics). *Russ. Geol. Geophys.* **2013**, *54*, 34–43. [[CrossRef](#)]

22. Kiseleva, O.N.; Zhmodik, S.M.; Damdinov, B.B.; Agafonov, L.V.; Belyanin, D.K. Composition and evolution of PGE mineralization in chromite ores from the Il'chir ophiolite complex (Ospa–Kitoi and Khara-Nur areas, East Sayan). *Russ. Geol. Geophys.* **2014**, *55*, 259–272. [[CrossRef](#)]
23. Kiseleva, O.; Zhmodik, S. PGE mineralization and melt composition of chromitites in Proterozoic ophiolite complexes of Eastern Sayan, Southern Siberia. *Geosci. Front.* **2017**, *8*, 721–731. [[CrossRef](#)]
24. Kiseleva, O.N.; Airiyants, E.V.; Belyanin, D.K.; Zhmodik, S.M. Podiform chromitites and PGE mineralization in the Ulan-Sar'dag ophiolite (East Sayan, Russia). *Minerals* **2020**, *10*, 141. [[CrossRef](#)]
25. Kiseleva, O.N.; Airiyants, E.V.; Belyanin, D.K.; Zhmodik, S.M. *Geochemical Features of Peridotites and Volcanogenic-Sedimentary Rocks of the Ultrabasic-Basitic Massif of Ulan Sar'dag (East Sayan, Russia)*; The Bulletin of Irkutsk State University: Irkutsk, Russia, 2019; (In Russian). [[CrossRef](#)]
26. Kiseleva, O.N.; Airiyants, E.V.; Belyanin, D.K.; Zhmodik, S.M.; Ashchepkov, I.V.; Kovalev, S.A. Multistage magmatism in ophiolites and associated metavolcanites of the Ulan-Sar'dag Mélange (East Sayan, Russia). *Minerals* **2020**, *10*, 1077. [[CrossRef](#)]
27. Fedorovskii, V.S.; Khain, E.V.; Vladimirov, A.G.; Kargopolov, S.A.; Gibsher, A.S.; Izokh, A.E. Tectonics, metamorphism, and magmatism of collisional zones of the Central Asian Caledonides. *Geotectonics* **1995**, *29*, 193–212.
28. Khain, E.; Gusev, G.S.; Khain, E.V.; Vernikovskiy, V.A.; Volobuev, M.I. Circum-Siberian Neoproterozoic Ophiolite Belt. *Ofioliti* **1992**, *22*, 195–200.
29. Sklyarov, E.V.; Kovach, V.P.; Kotov, A.B.; Kuzmichev, A.B.; Lavrenchuk, A.V.; Perelyaev, V.I.; Shchipansky, A.A. Boninites and ophiolites: Problems of their relations and petrogenesis of boninites. *Russ. Geol. Geophys.* **2016**, *57*, 127–140. [[CrossRef](#)]
30. Belyaev, V.A.; Wang, K.-L.; Gornova, M.A.; Dril, S.I.; Karimov, A.A.; Medvedev, A.Y.; Noskova, Y.V. Geochemistry and origin of the Eastern Sayan ophiolites, Tuva-Mongolian microcontinent (Southern Siberia). *Geodyn. Tectonophys.* **2017**, *8*, 411415. [[CrossRef](#)]
31. Wang, K.; Chu, Z.; Gornova, M.; Dril, S.; Belyaev, V.; Lin, K.; O'Reilly, S. Depleted SSZ type mantle peridotites in Proterozoic Eastern Sayan ophiolites in Siberia. *Geodyn. Tectonophys.* **2017**, *8*, 583–587. [[CrossRef](#)]
32. Belyaev, V.A. Boninite-tholeiite association in Mesoproterozoic Eastern Sayan ophiolites: Geochemistry and mineralogy of lavas, dikes, and cumulates. In Proceedings of the IX Siberian Conference of Young Scientists on Geosciences, Novosibirsk, Russia, 19–23 November 2018; Kruk, N.N., Yeltsov, I.N., Vernikovskiy, V.A., Eds.; V.S. Sobolev Institute of Geology and Mineralogy SB RAS, A.A. Trofimuk Institute of Oil and Gas Geology and Geophysics SB RAS, Novosibirsk State University: Novosibirsk, Russia, 2018; pp. 60–62. (In Russian).
33. Belyaev, V.A.; Gornova, M.A.; Wang, K.-L.; Korneva, A.P.; Karimov, A.A.; Medvedev, A.Y.; Dril, S.I.; Semiryakov, A.S.; Agasheva, E.A. Mezoproterozoic ophiolites of Eastern Sayan: U-Pb age of zircon (LA—ICP—MS) and geodynamic conditions of formation [abs.]. In Proceedings of the Russian Conference with International Participation on Dynamics and Interaction of the Earth's Geosphere, Tomsk State University, Tomsk, Russia, 8–11 November 2021; Tomsk Publisher House: Tomsk, Russia, 2021; pp. 232–233. (In Russian)
34. Gordienko, I.V.; Dobretsov, N.L.; Zhmodik, S.M.; Roschektayev, P.A. Multistage thrust and nappe tectonics on the southeastern part the eastern sayan and its role in the formation of large gold deposits. *Russ. Geol. Geophys.* **2021**, *62*, 109–120. [[CrossRef](#)]
35. Rudnev, S.N.; Gibsher, A.S.; Semenova, D.V. Vendian island arc intrusive magmatism of the Lake zone of Western Mongolia geological, geochronological, and petrochemical data). *Russ. Geol. Geophys.* **2021**, *62*, 619–632. [[CrossRef](#)]
36. Gibsher, A.S. Microcontinent of the Central Asian Mobile Belt. In Proceedings of the Conference on Geodynamic Evolution of the Central Asian Mobile Belt (from Ocean to Continent), Irkutsk, Russia, 17–20 October 2017; pp. 49–51. (In Russian).
37. Kuzmichev, A.; Kröner, A.; Hegner, E.; Liu, D.Y.; Wan, Y.S. The Shishkhid ophiolite, northern Mongolia: A key to the reconstruction of a Neoproterozoic island-arc system in central Asia. *Precambrian Res.* **2005**, *138*, 125–150. [[CrossRef](#)]
38. Travin, A.V.; Yudin, D.S.; Vladimirov, A.G.; Khromykh, S.V.; Volkova, N.I.; Mekhonoshin, A.S.; Kolotilina, T.B. Thermochronology of the Chernorud granulite zone, Ol'khon region, Western Baikal area. *Geochem. Int.* **2009**, *47*, 1107–1124. [[CrossRef](#)]
39. Baksi, A.K.; Archibald, D.A.; Farrar, E. Intercalibration of $^{40}\text{Ar}/^{39}\text{Ar}$ dating standards. *Chem. Geol.* **1996**, *129*, 307–324. [[CrossRef](#)]
40. Lee, J.-Y.; Marti, K.; Severinghaus, J.P.; Kawamura, K.; Yoo, H.-S.; Lee, J.B.; Kim, J.S. A redetermination of the isotopic abundances of atmospheric Ar. *Geochim. Cosmochim. Acta* **2006**, *70*, 4507–4512. [[CrossRef](#)]
41. Raczek, I.; Jochum, K.P.; Hofmann, A.W. Neodymium and strontium isotope data for USGS reference materials BCR-1, BCR-2, BHVO-1, BHVO-2, AGV-1, AGV-2, GSP-1, GSP-2 and eight MPI-DING reference glasses. *Geostand. Newsl.* **2003**, *27*, 173–179. [[CrossRef](#)]
42. Tanaka, T.; Togashi, S.; Hikari, K.; Hiroshi, A.; Hiroo, K.; Takuji, T.; Masaki Yu Yuji, O.; Shigekazu Yo Kunimaru, H.; Takahashi, T.; Yanagi, K.; et al. JNdi-1: A neodymium isotopic reference in consistency with LaJolla neodymium. *Chem. Geol.* **2000**, *168*, 279–281. [[CrossRef](#)]
43. Bouvier, A.; Vervoort, J.D.; Patchett, P.J. The Lu–Hf and Sm–Nd isotopic composition of CHUR: Constraints from unequilibrated chondrites and implications for the bulk composition of terrestrial planets. *Earth Planet. Sci. Lett.* **2008**, *273*, 48–57. [[CrossRef](#)]
44. Weis, D.; Kieffer, B.; Maerschalk, C.; Barling, J.; Jong, J.; Williams, G.A.; Hanano, D.; Pretorius, W.; Mattielli, N.; Scoates, J.S.; et al. High-precision isotopic characterization of USGS reference materials by TIMS and MCICP-MS. *Geochem Geophys Geosyst* **2006**, *7*, 139–149. [[CrossRef](#)]
45. Sun, S.S.; McDonough, W.F. Chemical and isotopic systematics of oceanic basalts; implications for mantle composition and processes. In *Magmatism in the Ocean Basins*; Saunders, A.D., Norry, M.J., Eds.; Geological Society: London, UK, 1989; Volume 42, pp. 313–345. [[CrossRef](#)]

46. Pearce, J.A.; Van der Laan, S.R.; Arculus, R.J.; Murton, B.J.; Ishii, T.; Peate, D.W.; Parkinson, I.J. Boninite and harzburgites from Leg 125 (Bonin-Mariana forearc): A case study of magma genesis during the initial stages of subduction. In Proceedings of the Ocean Drilling Program, 125, Scientific Results; Fryer, P., Pearce, J.A., Stokking, L.B., Ali, J.R., Arculus, R., Balotti, D., Burke, M.M., Ciampo, G., Haggerty, J.A., Haston, R.B., et al., Eds.; Ocean Drilling Program: College Station, TX, USA, 1992; Volume 125, pp. 623–659. [\[CrossRef\]](#)
47. Taylor, S.R.; McLennan, S.M. *The Continental Crust: Its Evolution and Composition*; Blackwell: London, UK, 1985; 312p.
48. Jacobsen, S.B.; Wasserburg, G.J. Sm-Nd evolution of chondrites and achondrites. *Earth Planet. Sci. Lett.* **1984**, *67*, 137–150. [\[CrossRef\]](#)
49. Faure, G. *Principles of Isotope Geology*, 2nd ed.; Wiley and Sons: New York, NY, USA, 1986; 589p.
50. Taylor, H.P. The effect of assimilation of rocks by magmas: $^{18}\text{O}/^{16}\text{O}$ and $^{87}\text{Sr}/^{86}\text{Sr}$ systematics in igneous rocks. *Earth Planet. Sci. Lett.* **1980**, *47*, 243–254. [\[CrossRef\]](#)
51. Pokrovsky, B.G. *Crustal Contamination of Mantle Magmas According to Isotope Geochemistry*; Nauka: Moscow, Russia, 2000; p. 225. (In Russian)
52. Kuznetsov, A.B.; Ovchinnikova, G.V.; Gorokhov, I.M.; Vasil'eva, I.M.; Gorokhovskii, B.M.; Semikhatov, M.A.; Kaurova, O.K.; Krupenin, M.T.; Maslov, A.V. The Sr isotopic characterization and Pb-Pb age of carbonate rocks from the Satka formation, the lower Riphean Burzyan group of the Southern Urals. *Stratigr.* **2008**, *16*, 120–137. [\[CrossRef\]](#)
53. Kuznetsov, A.B.; Letnikova, E.F.; Vishnevskaya, I.A.; Konstantinova, G.V.; Kutyavin, E.P.; Geletiy, H.K. Sr chemostratigraphy of carbonate sedimental cover of the Tuvino-Mongolsk microcontinent. *Dokl. Earth Sci.* **2010**, *432*, 350–355. [\[CrossRef\]](#)
54. Kovach, V.P.; Kotov, A.B.; Terent'eva, L.B.; Yarmolyuk, V.V.; Kovalenko, V.I.; Kozlovskiy, A.M. Composition, sources, and mechanisms of formation of the continental crust of the Lake zone of the Central Asian caledonides. II. Geochemical and Nd isotope data. *Petrology* **2011**, *19*, 399–425. [\[CrossRef\]](#)
55. Munker, C.; Worner, G.; Yogodzinski, G.M.; Churicova, T.G. Behaviour of high field strength elements in subduction zone: Constrains from Kamchatka-Aleutian arc lavas. *Earth Planet. Sci. Lett.* **2004**, *224*, 275–293. [\[CrossRef\]](#)
56. Kovach, V.P.; Kozakov, I.K.; Kroner, A.; Salnikova, E.; Wang, K.-L.; Lee, H.-Y.; Chung, S.-L. Early Neoproterozoic crust formation in the Dzabkhan microcontinent, Central Asian Orogenic Belt. *Geodynam. Tectonophys.* **2017**, *8*, 499–501. [\[CrossRef\]](#)
57. DePaolo, D.J.; Wasserburg, G.J. The sources of island arcs as indicated by Nd and Sr isotopic studies. *Geophys. Res. Lett.* **1977**, *4*, 465–468. [\[CrossRef\]](#)
58. Whitford, D.J.; Compston, W.; Nicholls, I.A.; Abbot, M.J. Geochemistry of late Cenozoic lavas from eastern Indonesia: Role of subducted sediments in petrogenesis. *Geology* **1977**, *5*, 571–575. [\[CrossRef\]](#)
59. Vorontsov, A.; Yarmolyuk, V.; Fedoseev, G.; Nikiforov, A.; Sandimirova, G. Isotopic and Geochemical Zoning of Devonian Magmatism in the Altai-Sayan Rift System: Composition and Geodynamic Nature of Mantle Sources. *Petrology* **2010**, *18*, 596–609. [\[CrossRef\]](#)
60. Kröner, A.; Kovach, V.; Alexeiev, D.; Wang, K.-O.; Wong, J.; Degtyarev, K.; Kozakov, I. No excessive crustal growth in the Central Asian Orogenic Belt: Further evidence from field relationships and isotopic data. *Gondwana Res.* **2017**, *50*, 135–166. [\[CrossRef\]](#)
61. Turkina, O.M.; Sukhorukov, V.P.; Sergeev, S.A. Mesoarchean bimodal volcanic rocks of the Onot greenstone belts, southwestern Siberian craton: Implications for magmatism in an extension/rift setting. *Precambrian Res.* **2020**, *343*, 105731. [\[CrossRef\]](#)
62. Kovalenko, V.I.; Yarmolyuk, V.V.; Kovach, V.P.; Kotov, A.B.; Sal'nikova, E.B. Magmatism and geodynamics of early Caledonian structures of the Central Asian fold belt (isotopic and geological data). *Russ. Geol. Geophys.* **2003**, *12*, 1235–1248.
63. Jahn, B.M.; Wu, F.; Chen, B. Massive granitoid generation in Central Asia: Nd isotope evidence and implication for continental growth in the Phanerozoic. *Episodes* **2000**, *23*, 82–92. [\[CrossRef\]](#)
64. Zindler, A.; Hart, S.R.; Brooks, C. The Shabogamo Intrusive Suite, Labrador: Sr and Nd isotopic evidence for contaminated mafic magmas in the Proterozoic. *Earth Planet. Sci. Lett.* **1981**, *54*, 217–235. [\[CrossRef\]](#)
65. Amelin Yu, V.; Neymark, L.A.; Ritsk EYu Nemchin, A.A. Enriched Nd–Sr–Pb Isotopic Signatures in the Dovyren Layered Intrusion (Eastern Siberia, Russia): Evidence for Contamination by Ancient Upper Crustal Material. *Chem. Geol.* **1996**, *129*, 39–69. [\[CrossRef\]](#)
66. Ishizaka, K.; Karlson, R.W. Nd-Sr systematics of t11e Setouchi volcanic rocks, southwest Japan: A clue to the origin of orogenic andesites. *Earth Planet. Sci. Lett.* **1983**, *64*, 327–340. [\[CrossRef\]](#)
67. McCulloch, M.T.; Perfit, M.R. $^{143}\text{Nd}/^{144}\text{Nd}$, $^{87}\text{Sr}/^{86}\text{Sr}$ and trace element constraints on the petrogenesis of Aleutian island arc magmas. *Earth Planet. Sci. Lett.* **1981**, *56*, 167–179. [\[CrossRef\]](#)
68. Schaaf, P.; Heinrich, W.; Besch, T. Composition and Sm-Nd isotopic data of the lower crust beneath San Luis Potosi, Central Mexico: Evidence from granulite-facies xenolith suite. *Chem Geol.* **1994**, *118*, 63–84. [\[CrossRef\]](#)
69. Kempton, P.D.; Harmon, R.S.; Hawkesworth, C.J.; Moorbath, S. Petrology and geochemistry of lower crustal granulites from the Geronimo Volcanic Field, southern Arizona. *Geochim. Cosmochim. Acta* **1990**, *54*, 3401–3426. [\[CrossRef\]](#)
70. Zindler, A.; Hart, S. Chemical geodynamics. *Annu. Rev. Earth Planet. Sci.* **1986**, *14*, 493–571. [\[CrossRef\]](#)
71. Hart, S.R. Heterogeneous mantle domains: Signatures, genesis, and mixing chronologies. *Earth Planet. Sci. Lett.* **1988**, *90*, 273–296. [\[CrossRef\]](#)
72. Pe-Piper, G. The nature of Triassic extension-related magmatism in Greece: Evidence from Nd and Pb isotope geochemistry. *Geol. Magaz.* **1998**, *135*, 331–348. [\[CrossRef\]](#)

73. Gianni, G.M.; Lujan, S.P. Geodynamic controls on magmatic arc migration and quiescence. *Earth Sci. Rev.* **2021**, *218*, 103676. [[CrossRef](#)]
74. Sisson, V.B.; Pavlis, T.L.; Roeske, S.M.; Thorkelson, D.J. Introduction: An overview of ridge-trench interactions in modern and ancient settings. *Geol. Soc. Am. Spec. Pap.* **2003**, *371*, 1–18.
75. Rabayrol, F.; Hart, C.J.R.; Thorkelson, D.J. Temporal, spatial and geochemical evolution of late Cenozoic post-subduction magmatism in central and eastern Anatolia, Turkey. *Lithos* **2019**, *336–337*, 67–96. [[CrossRef](#)]
76. Vescheva, S.V.; Turkina, O.M.; Letnikova, E.F.; Ronkin, Y.L. Geochemical and Sm–Nd isotopic characteristics of the Neoproterozoic terrigenous rocks of the Tuva–Mongolian Massif. *Dokl. Earth Sci.* **2008**, *418*, 155–160. [[CrossRef](#)]
77. Kovach, V.P.; Jian, P.; Yarmolyuk, V.V.; Kozakov, I.K.; Liu, D.; Terent'eva, L.B.; Lebedev, V.I.; Kovalenko, V.I. Magmatism and geodynamics of early stages of the Paleo Asian ocean formation: Geochronological and geochemical data on ophiolites of the Bayan-Khongor zone. *Doklady Earth Sci.* **2005**, *404*, 1072–1077.
78. Fitton, J.G.; Saunders, A.D.; Norry, M.J.; Hardarson, B.S.; Taylor, R.N. Thermal and chemical structure of the Iceland plume. *Earth Planet. Sci. Lett.* **1997**, *153*, 197–208. [[CrossRef](#)]
79. Gordienko, I.V.; Metelkin, D.V. The evolution of the subduction zone magmatism on the Neoproterozoic and Early Paleozoic active margins of the Paleoasian Ocean. *Russ. Geol. Geophys.* **2016**, *57*, 69–81. [[CrossRef](#)]
80. Gordienko, I.V. Relationship between subduction-related and plume magmatism at the active boundaries of lithospheric plates in the interaction zone of the Siberian continent and Paleoasian Ocean in the Neoproterozoic and Paleozoic. *Geodyn. Tectonophys.* **2019**, *10*, 405–457. [[CrossRef](#)]